TM-71-1022-7

# TECHNICAL MEMORANDUM

## APPLICATION OF STATISTICAL COMMUNICATION THEORY TO THE PERFORMANCE ANALYSIS OF THE S-192 MULTISPECTRAL SCANNER



Bellcomm

BELLCOMM, INC.
955 L'ENFANT PLAZA NORTH, S.W., WASHINGTON, D.C. 20024

## COVER SHEET FOR TECHNICAL MEMORANDUM

TITLE- Application of Statistical Communication Theory to the Performance Analysis of the S-192 Multispectral Scanner

TM- 71-1022-7

DATE- December 30, 1971

FILING CASE NO(S)- 620

AUTHOR(S)- R. J. Ravera

FILING SUBJECT(S) (ASSIGNED BY AUTHOR(S))- Infrared Scanner
Line Scanning Image System
Multispectral Scanner
Skylab Experiments

ABSTRACT

The performance of the S-192 Multispectral Scanner is evaluated using the principles of modern communication theory. This method permits a unified treatment of the interrelated design questions of detector noise and frequency response, aperture size and scan rate, digital sampling, and system transient response.

Quantitative estimates of expected performance are given for the class of ground radiance functions whose auto-correlation functions are exponential in the radius. Detector performance is treated parametrically and other system parameters have their design values.

The principal results are:

1. The optimum sampling rate for a channel whose detector just meets the noise specification is 1.3 samples per Instantaneous Field of View (IFOV).

2. The present S-192 design sampling rate for five of the thirteen channels is 1.1 samples per IFOV. Because the total system error has a shallow minimum, the design sampling rate is close to optimum. This result is in opposition to the view held in some quarters that the S-192 system is digital data bandwidth limited.

3. Sampling the remaining eight channels at a rate of 2.2 samples per IFOV does not improve system performance.



SEE REVERSE SIDE FOR DISTRIBUTION LIST

Bellcomm

955 L'Enfant Plaza North, S.W.
Washington, D. C. 20024

date: December 30, 1971

to: Distribution

TM-71-1022-7

from: R. J. Ravera

subject: Application of Statistical Communication Theory to the Performance Analysis of the S-192 Multispectral Scanner - Case 620

TECHNICAL MEMORANDUM

## 1.0 INTRODUCTION

### 1.1 General

This paper is devoted to the application of the principles of modern statistical communication theory to the performance analysis of the S-192 Multispectral Scanner system. This method enjoys the advantage of providing a unified treatment of the interrelated design questions of detector noise and frequency response, aperture size and scan rate, digital sampling rate, and system transient response. In order to provide a basis for a parametric study, a system performance measure must be established. Image quality, that is the ability of the system to accurately view, record, and reconstruct a given ground scene, is the qualitative description of system performance. The basic difference between the approach used in this paper and current practice for S-192 is the method of quantifying or measuring image quality.

## 1.2 Current S-192 System Performance Specification

One specification of image quality for S-192 is Noise Equivalent change in Reflectance (NE$\Delta\rho$). The End Item Specification for S-192 [1]* places an upper limit on NE$\Delta\rho$ for the first 12 bands of 1.0%.** In its narrowest interpretation, NE$\Delta\rho$ can be restricted to be a measure of detector performance only [2]. The wider interpretation of NE$\Delta\rho$ can include such overall system properties as detector electronics (including boost circuits, filters, preamplifiers) and noise sources other than the detector itself [3,4]. Basically, NE$\Delta\rho$ is an inverse signal-to-noise ratio and it represents an important first step in estimating required detector properties. Its major limitation as a measure of system performance is that, by itself, it is not flexible enough to provide the kind of trade-off capability required in design and analysis. For example, NE$\Delta\rho$ can be easily reduced by providing stronger post detector filtering. However, such improvement in NE$\Delta\rho$ is taken at the expense of the system fidelity capability. NE$\Delta\rho$ does not provide a proper trade-off point. To insure fidelity, the NE$\Delta\rho$ specification can be supplemented with some specification on system bandwidth properties, as is done for S-192. It is not easy to do this quantitatively with the trade-off clearly visible.

## 1.3 Proposed Approach

The most general approach to quantifying image quality would appear to be a comparison of the actual system input with

---

*Square brackets indicate References.

**The thirteenth band is the thermal band and will not be considered here.

system output, and this is usually carried out in a mean squared sense. That is, if $T(x,y)$ is the actual radiance of the ground scene and $T'(x,y)$ is the radiance as viewed, recorded and reconstructed by the system, then a normalized error, $\bar{\varepsilon}$, is defined by

$$\bar{\varepsilon} = \left[ \lim_{X,Y\to\infty} \frac{1}{XY} \frac{1}{\bar{T}^2} \int_{-X/2}^{X/2} \int_{-Y/2}^{Y/2} [T(x,y)-T'(x,y)]^2 dxdy \right]^{1/2} \quad (1.1)$$

where $\bar{T}$ is the mean ground radiance. Eq. (1.1) represents the classical mathematical definition of a normalized root mean squared (rms) error and all reference in this paper to rms error is based on Eq. (1.1). If the system input were deterministic, Eq. (1.1) could be used directly. However, it is indicated in Section 3.2 that a stochastic model of ground radiance appears to be more desireable and is therefore employed. Thus, auto-correlation functions, Fourier analysis and power spectral density functions must be introduced to evaluate Eq. (1.1). Application of the latter techniques to electro-optical systems has a strong technical foundation [5,6,7,8,9].

## 1.4 Organization

Section 2 defines the terms and introduces the concepts required for the theoretical analysis in Section 3.3. Sections 3.1 and 3.2 are general descriptions of the system model. Section 4 discusses the details of the actual S-192 system components and Sections 5 and 6 contain, respectively, the results and conclusions. For the reader not interested in the detailed theoretical analysis, it is necessary to read only Sections 3.1 and 3.2, Section 4.11, Section 5, and Section 6.

## 2.0 REVIEW OF CONCEPTS AND DEFINITIONS

### 2.1 Fourier Transform Pair

The two dimensional Fourier transform pair used in this paper is:

$$\left.\begin{aligned} H(k_x,k_y) &= \int_{-\infty}^{\infty}\int h(x,y)e^{-2\pi j(k_x x+k_y y)}\,dxdy \\ \text{and} \\ h(x,y) &= \int_{-\infty}^{\infty}\int H(k_x,k_y)e^{2\pi j(k_x x+k_y y)}\,dk_x dk_y \end{aligned}\right\} \qquad (2.1)$$

The following notation will also be employed:

$$H(k_x,k_y) = F\{h(x,y)\}$$

$$h(x,y) = F^{-1}\{H(k_x,k_y)\}$$

### 2.2 Unit Impulse and Impulse Response Functions

The unit impulse function, also termed the Dirac delta function, $\delta(x,y)$, is defined by

$$\int_{-\infty}^{\infty}\int \delta(x-x_0,y-y_0)f(x,y)\,dxdy = f(x_0,y_0) \qquad (2.2)$$

For more details see, for example, Papoulis [10].

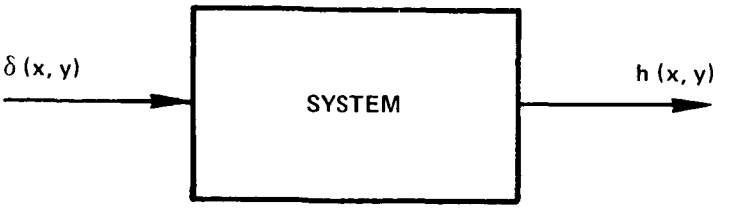


FIGURE 2.1

If we subject a system or a component of the system to a unit impulse function as shown in Figure 2.1, then the output is termed the impulse response function, h(x,y). The impulse response function has the following property.

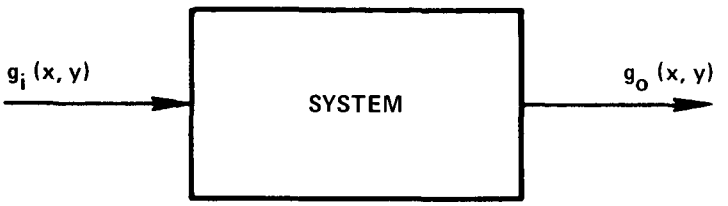


FIGURE 2.2

If h(x,y) is the impulse response function of the system in Figure 2.2, and the system is subjected to an input $g_i(x,y)$ then the output is [10]

$$g_0(x,y) = \int_{-\infty}^{\infty}\int g_i(\xi,\eta)h(x-\xi,y-\eta)d\xi d\eta \qquad (2.3)$$

It is therefore sufficient to represent a system by its impulse response function.

## 2.3 System Transfer Function

A system or a system component may also be represented by its transfer function. The transfer function is simply the Fourier transform of the impulse response function. Thus, if $h(x,y)$ is the impulse response function, the system transfer function, $H(k_x,k_y)$, is from Eq. (2.1)

$$H(k_x,k_y) = F\{h(x,y)\} = \int_{-\infty}^{\infty}\int h(x,y)e^{-2\pi j(k_x x+k_y y)}dxdy \tag{2.4}$$

The advantage of representing a system by its transfer function, in certain cases, will be shown later.

## 2.4 Autocorrelation Function

The autocorrelation function, $A_g(x,y)$, of a variable $g(x,y)$ is defined as

$$A_g(x,y) = \lim_{X,Y\to\infty} \frac{1}{XY} \int_{-X/2}^{X/2}\int_{-Y/2}^{Y/2} g(\xi,\eta)g(\xi+x,\eta+y)d\xi d\eta \tag{2.5}$$

Autocorrelation functions are most often used to describe random variables [9]. Note the important property that

$$A_g(0,0) = \lim_{X,Y\to\infty} \frac{1}{XY} \int_{-X/2}^{X/2}\int_{-Y/2}^{Y/2} g(\xi,\eta)^2 d\xi d\eta = \overline{g^2} \tag{2.6}$$

where $\overline{g^2}$ is the mean square value of $g(x,y)$, assumming the mean square value exists. An alternate representation for $A_g(x,y)$ is

$$A_g(x,y) = E\{gg_+\} \tag{2.7}$$

where E{ } represents the "expected value" operation and the "+" subscript indicates that the second g is incremented (just as in Eq. 2.5).

2.5 Crosscorrelation Function

The crosscorrelation function of two variables, g(x,y) and f(x,y), is defined by

$$C_{g_+f} = \lim_{X,Y\to\infty} \frac{1}{XY} \int_{-X/2}^{X/2} \int_{-Y/2}^{Y/2} g(\xi+x,\eta+y) f(\xi,\eta) d\xi d\eta \qquad (2.8)$$

where the "+" subscript after the g indicates the incremented variable. An equivalent representation is

$$C_{g_+f} = E\{g_+ f\} \qquad (2.9)$$

2.6 Power Spectral Density Function

The power spectral density function (PSD), $P_g(k_x,k_y)$, of a variable g(x,y) is defined as the Fourier transform of the autocorrelation function of g(x,y); thus,

$$P_g(k_x,k_y) = F\{A_g(x,y)\} = \int_{-\infty}^{\infty}\int A_g(x,y) e^{-2\pi j(k_x x+k_y y)} dxdy \qquad (2.10)$$

As mentioned in Section 2.5, the autocorrelation function, and hence the PSD function, are usually associated with stochastic variables rather than deterministic variables. The term "power" in PSD does not in general indicate that the PSD function has units of mechanical or electrical power. A good physical interpretation of PSD is given by Lee [6]. From Eqs. (2.10) and (2.1)

$$A_g(x,y) = \int_{-\infty}^{\infty}\int P_g(k_x,k_y)e^{2\pi j(k_x x+k_y y)}dk_x dk_y \tag{2.11}$$

Combining Eqs. (2.11) and (2.6) leads to an alternate way of determining the mean square value of g(x,y):

$$\overline{g^2} = A_g(0,0) = \int_{-\infty}^{\infty}\int P_g(k_x,k_y)dk_x dk_y \tag{2.12}$$

A cross-power spectral density function can also be defined;

$$P_{g_+f}(k_x,k_y) = F\{C_{g_+f}(x,y)\}.$$

## 2.7 Further Input/Output Relationships

Eq. (2.3) is a direct input/output relationship which is advantageous when dealing with deterministic variables. Stochastic variables, however, are represented by correlation and/or PSD functions and it is therefore helpful to write down the input/output relations governing these quantities. If the input variable $g_i(x,y)$ of Figure 2.2 has an autocorrelation function $A_{g_i}(x,y)$ then it can be shown that [6,8]

$$A_{g_o}(x,y) = A_{g_i}(x,y)*h(x,y)*h(-x,-y) \tag{2.13}$$

where h(x,y) is the impulse response function of the system and the asterisk represents the convolution operation; i.e.,

$$g(x,y)*h(x,y) = \int_{-\infty}^{\infty}\int g(\xi,\eta)h(x-\xi,y-\eta)d\xi d\eta$$

It may also be shown that [8,9]

$$C_{g_{i+}g_o} = A_{g_i}(x,y)*h(-x,-y) \tag{2.14}$$

and

$$C_{g_ig_{o+}} = A_{g_i}(x,y)*h(x,y) \tag{2.15}$$

The corresponding input/output relationships for the PSD functions are found by taking the Fourier transform of Eqs. (2.13), (2.14) and (2.15):

$$P_{g_o} = P_{g_i}|H(k_x,k_y)|^2 \tag{2.16}$$

$$P_{g_{i+}g_o} = P_{g_i}\bar{H}(k_x,k_y) \tag{2.17}$$

and

$$P_{g_ig_{o+}} = P_{g_i}H(k_x,k_y) \tag{2.18}$$

where $H(k_x,k_y)$ is the transfer function of the system and the bar over a function represents the complex conjugate unless otherwise stated. The advantage of the use of the PSD - transfer function representation over that of the corresponding correlation relationship is that one substitutes multiplication for convolution.

## 2.8 Sampled Functions

A few properties of sampled functions are required for the analysis of the scanning system. Some of these properties are derived by various methods in References 10, 11 and 12. They are rederived in Appendices A and B using a more unified approach. For simplicity functions of a single variable will be discussed; the extension to functions of two or more variables is straightforward. It is assumed that a function which is sampled at discrete intervals, a distance $t_i$ apart, may be represented by

$$g(\tilde{t}) = \sum_{n=-\infty}^{\infty} g(t)\delta(t/t_i - n) \tag{2.19}$$

where the tilde over the t indicates that g(t) is sampled at discreet values of t. (The advantage of this notation becomes clear when sampling functions of two or more variables.) Based on Eq. (2.19) the following properties of sampled functions are derived in Appendix A. If a sampled function $g(\tilde{t})$ can be represented by Eq. (2.19), then its autocorrelation function $E\{g(\tilde{t})_+ g(\tilde{t})\}$, takes the form

$$A_g(\tilde{t}) = E\{g(\tilde{t})_+ g(\tilde{t})\} = \sum_{n=-\infty}^{\infty} A_g(t)\delta(t/t_i - n) \tag{2.20}$$

where $A_g(t)$ is the autocorrelation function of g(t).
The crosscorrelation function of a sampled function $g(\tilde{t})$ and a non-sampled function h(t) can be shown to be equal to the crosscorrelation function of the unsampled functions g(t) and h(t); that is (Eq. (A-17))

$$E\{g(\tilde{t})_+ h(t)\} = C_{g_+h}(t) \tag{2.21}$$

Setting g(t) = h(t) in Eq. (2.21) gives

$$E\{g(\tilde{t})_+ g(t)\} = C_{g_+g}(t) = A_g(t) \tag{2.22}$$

As a result of Eqs. (2.20), (2.21) and (2.22), the following identities are established in Appendix B. The PSD function, $\tilde{P}_g(f)$, of a sampled variable $g(\tilde{t})$ can be written in terms of of the autocorrelation function as (Eq. (B-6))

$$\tilde{P}_g(f) = \sum_{m=-\infty}^{\infty} A_g(mt_i)e^{-2\pi jmft_i}\, t_i \qquad (2.23)$$

where f is the Fourier transform variable associated with t and $t_i$ is the interval between samples. The mean square value, $\overline{g^2(\tilde{t})}$, of a sampled function $g(\tilde{t})$ can be found from (Eq. (B-9))

$$\overline{g^2(\tilde{t})} = \int_{-1/2t_i}^{1/2t_i} \tilde{P}_g(f)\,df \qquad (2.24)$$

Finally, the relationship between the PSD function of a sampled quantity $g(\tilde{t})$ and the PSD of its non-sampled generator g(t) is (Eq. (B-14))

$$\tilde{P}_g(f) = \sum_{m=-\infty}^{\infty} P_g(f-m/t_i) \qquad (2.25)$$

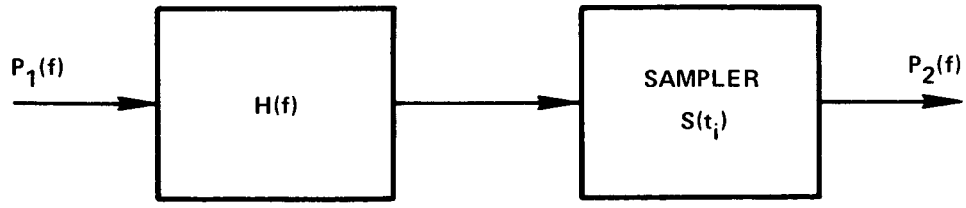


FIGURE 2.3

As a result of Eqs. (2.16) and (2.25) the input/output relationship of the system shown in Figure 2.3 is

$$P_2(f) = \sum_{m=-\infty}^{\infty} P_1(f-m/t_i) \left| H(f-m/t_i) \right|^2 \tag{2.26}$$

Also, assuming that the signal entering H(f) in Figure 2.3 is not sampled, Eqs. (2.21), (2.17) and (2.18) yield

$$P_{21_+}(f) = P_1(f)\bar{H}(f) \tag{2.27}$$

and

$$P_{2_+1}(f) = P_1(f)H(f) \tag{2.28}$$

On the other hand, if a sampler did exist before H(f), then it can be demonstrated that

$$P_{21_+}(f) = \sum_{m=-\infty}^{\infty} P_1(f-\frac{m}{t_i})\bar{H}(f-\frac{m}{t_i}) \tag{2.29}$$

and

$$P_{2_+1}(f) = \sum_{m=-\infty}^{\infty} P_1(f-\frac{m}{t_i})H(f-\frac{m}{t_i}) \tag{2.30}$$

## 3.0 SYSTEM MODEL AND ANALYSES

### 3.1 General

Figure 3.1 is a representation of the S-192 scanning system as it operates aboard the spacecraft. The ground track of the spacecraft is the y-direction and the cross-track direction is the x-direction. The values of the various parameters in Figure 3.1 are consistent with the S-192 multispectral scanner. The upper loop of Figure 3.2 represents the model of the line scanning image system used to represent the S-192 system. The $H_1$, $H_2$, $H_3$ and $H_4$ are the transfer functions of the major system components. The $k_x$ and $k_y$ are the spatial frequencies (cycles/ft) associated with the Fourier transform. The action of the x-scanner and y-sampler converts the two dimensional signal, T(x,y) into a one dimensional analog signal. The scan rate v can be used to transfer the electrical component's dependency on temporal frequency f(Hz) to dependency on $k_x$.

As the spacecraft moves over its ground track, the target radiance, T(x,y), passes through an aperture $H_1$ which scans in the cross-track direction. The circular scanning operation is carried out such that concentric bands of the ground are scanned. However, since data are taken only over 120° of the scan circle (See Figure 3.1), it is assumed that there is a linear scan in the x-direction at a constant value of y. Hence the total effect of this operation is to scan in x and sample in y. The radiance signal is then relayed to the detector, $H_2$, which converts it to an electrical signal. Various electronics (boost circuit, filter, etc.) follow the detector and are lumped in $H_3$. The output of $H_3$ is then prepared for digital recording on tape. This involves sampling in time (or equivalently, x) and quantization. At some later

WIDE-RANGE IR IMAGER INTEGRATION REQUIREMENTS

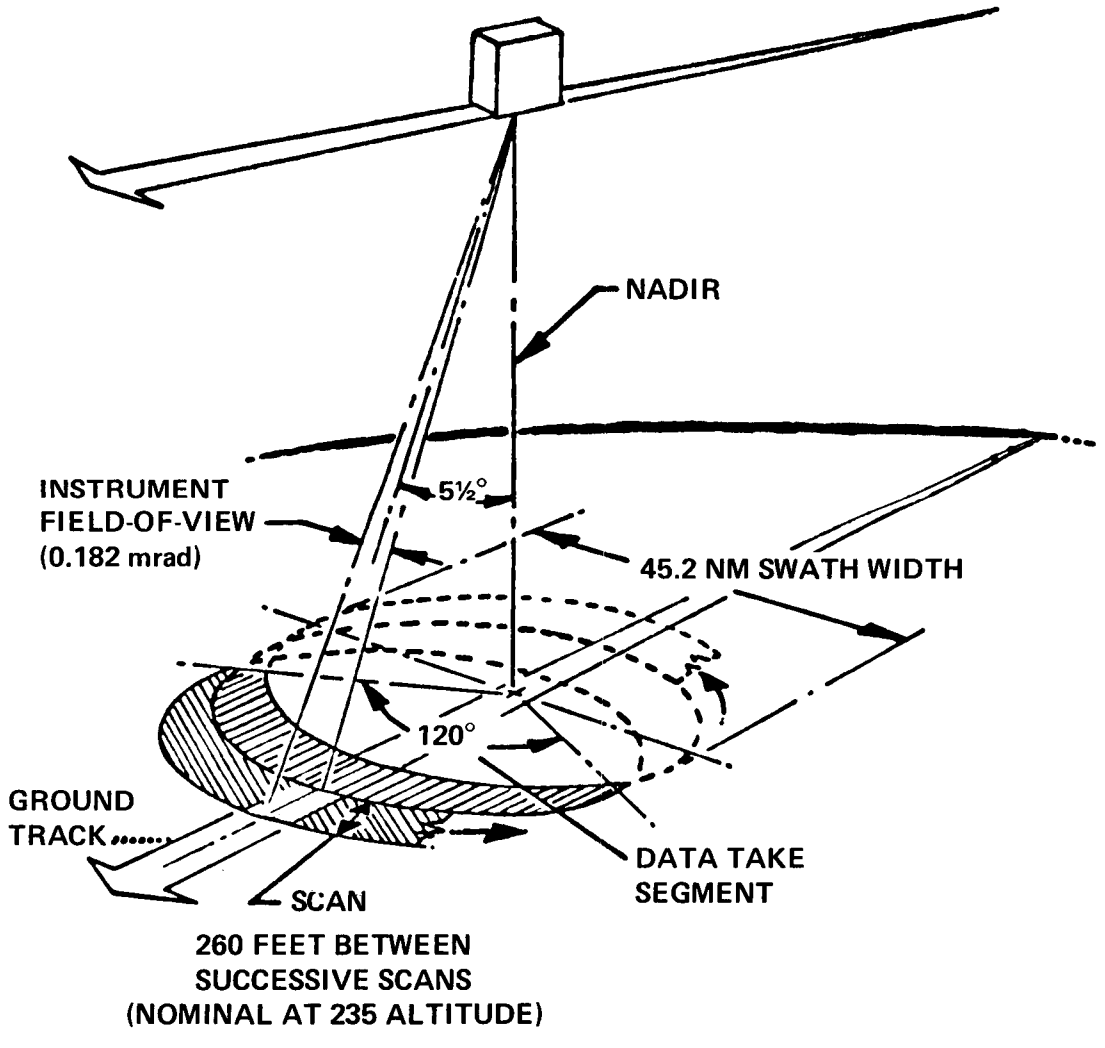


FIGURE 3.1

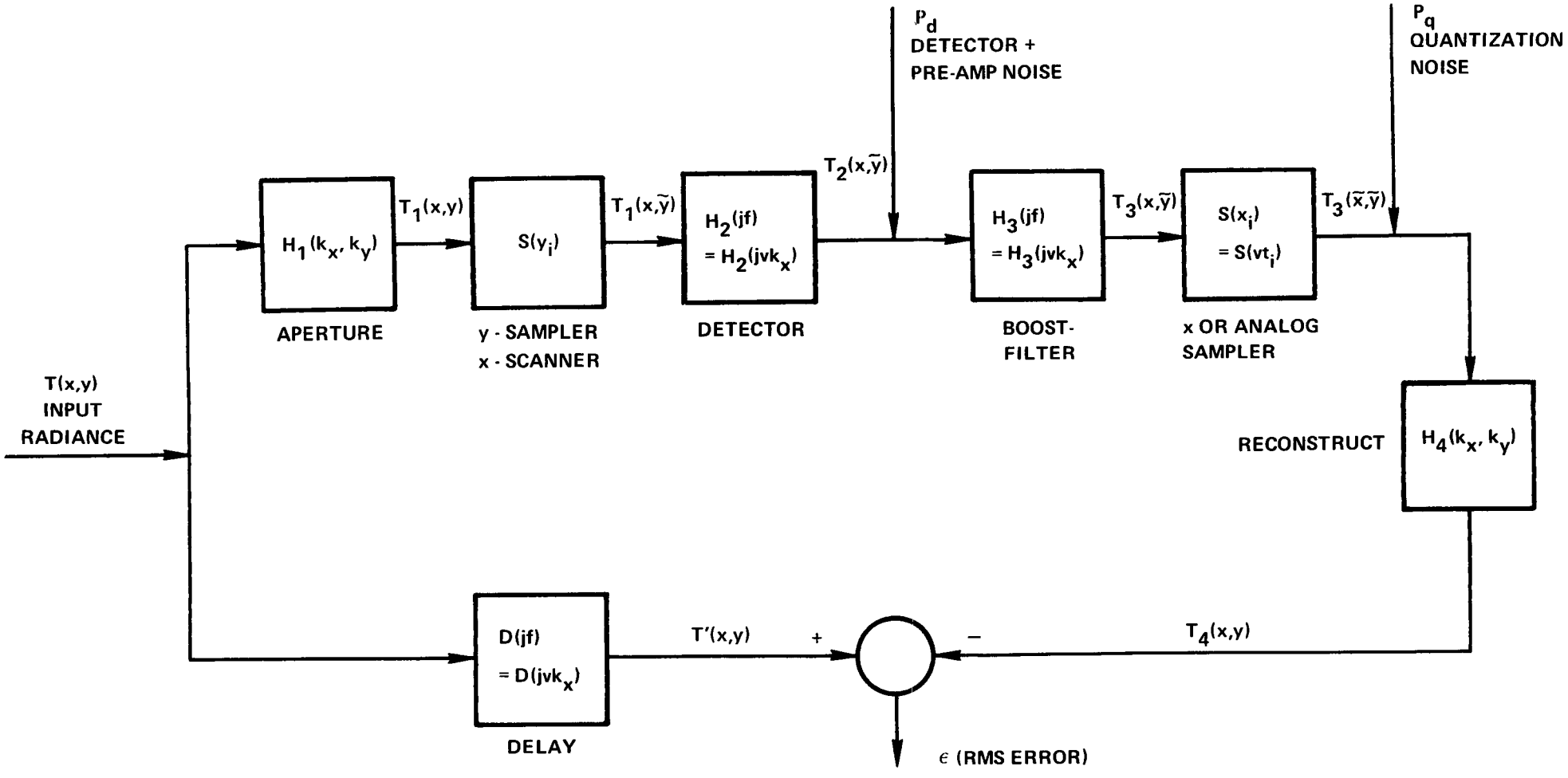
$P_d$
DETECTOR +
PRE-AMP NOISE
$P_q$
QUANTIZATION
NOISE
$H_1(k_x, k_y)$
APERTURE
$T_1(x,y)$
$S(y_i)$
y - SAMPLER
x - SCANNER
$T_1(x,\tilde{y})$
$H_2(jf)$
$= H_2(jvk_x)$
DETECTOR
$T_2(x,\tilde{y})$
$H_3(jf)$
$= H_3(jvk_x)$
BOOST-
FILTER
$T_3(x,\tilde{y})$
$S(x_i)$
$= S(vt_i)$
x OR ANALOG
SAMPLER
$T_3(\tilde{x},\tilde{y})$
T(x,y)
INPUT
RADIANCE
RECONSTRUCT
$H_4(k_x, k_y)$
D(jf)
$= D(jvk_x)$
DELAY
T'(x,y)
+
–
$T_4(x,y)$
$\epsilon$ (RMS ERROR)

FIGURE 3.2

time, this sampled signal is passed through a reconstruction filter, $H_4$, which will retrieve the system's representation of the original ground radiance scene.

The lower loop in Figure (3.2) completes the closed loop model which is used to compute the scanning system error. If the delay were not present in the lower loop, the signal delay, $t_d$, through the upper loop would cause us to compare two different ground "pictures" taken $t_d$ seconds apart, adding unnecessarily to the error. Thus, the lower loop is delayed by $t_d$ seconds.

Note in Figure 3.2 that detector, preamplifier and quantization noise are added to the system at the appropriate points. Details of the various transfer functions and noise power spectra are discussed in Section 4.0.

## 3.2 Ground Radiance Model

An important aspect of this kind of study is to devise an appropriate ground radiance model to represent T(x,y). The representation of T(x,y) will also impact the analysis; for example, T(x,y) may be deterministic or stochastic. One would like to have the flexibility of incorporating the randomness of ground detail found in nature and it therefore seems that the stochastic approach is the most appropriate. In analogous situations, for example, when modeling gust velocities or height variations on airport runways, an autocorrelation function for the a.c. component of the quantity of interest is assumed to take the form

$$A(x,y) = e^{-\alpha (x^2+y^2)^{1/2}}$$

In Reference 9, such a form for ground radiance is employed and the authors attribute this model to R. C. Clark. The complete expression for the autocorrelation of the a.c. component of ground radiance used in this paper is identical to the Clark model:

$$A_T(x,y) = e^{-\frac{\ln 2}{x_T}(x^2+y^2)^{1/2}} \tag{3.1}$$

The parameter $x_T$ may be thought of as a quantitative distance measure between varying ground radiance values. Two important properties of this model are apparent. First, since Eq. (3.1) represents the a.c. component only, the variance of $T(x,y)$, $\sigma_T^2$, is given by

$$\sigma_T^2 = E\{(T-\bar{T})^2\} = A_T(0,0) = 1 \tag{3.2}$$

where $\bar{T}$ is the mean value of the target radiance. Second, when $x_T = (x^2+y^2)^{1/2}$, $A_T(x,y) = 1/2$.

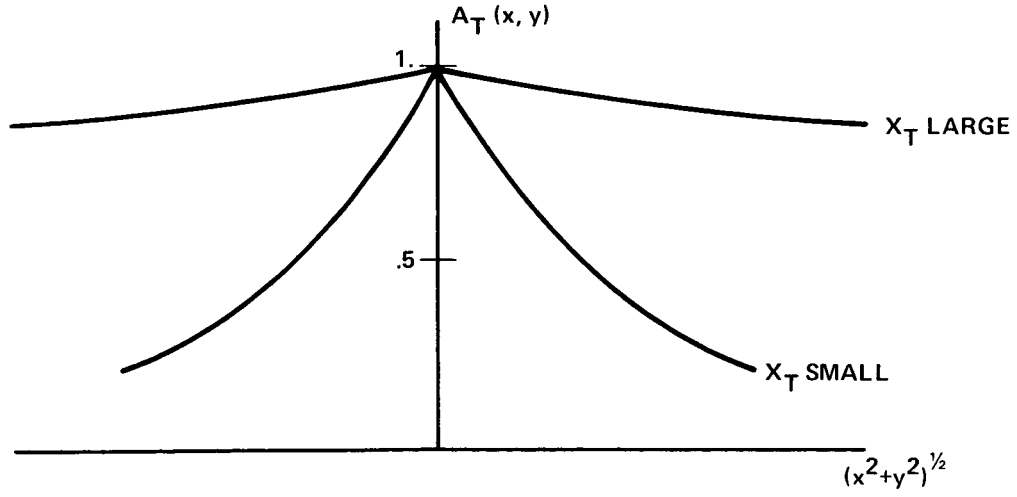


FIGURE 3.3

As illustrated in Figure 3.3, a large value of $x_T$ causes $A_T(x,y)$ to decrease slowly, indicating good point to point correlation of radiance values on the ground. Thus, a large $x_T$ would be appropriate, for example, when one wishes to represent desert areas where ground detail is generally uniform over large distances. For small $x_T$ the autocorrelation function drops off rapidly indicating less point to point correlation. This might occur, for example, when flying over suburban areas which contain built up sections alternating with open fields and/or wooded areas. Taking the Fourier transform of Eq. (3.1) gives the PSD of the a.c. component of ground radiance:

$$P_T(k_x,k_y) = \left(\frac{1}{2\pi}\right)^2 \frac{\ln 2}{x_T} \frac{1}{\left[k_x^2+k_y^2+\left(\frac{\ln 2}{2\pi x_T}\right)^2\right]^{3/2}} \tag{3.3}$$

It follows from Eqs. (2.12) and (3.2) and may be verified by direct integration that

$$\sigma_T^2 = \int_{-\infty}^{\infty}\int P_T(k_x,k_y)\,dk_x\,dk_y = 1.$$

## 3.3 Analysis of the Model

Having established the model for the ground radiance function $T(x,y)$, the method of analysis is now fixed. The fact that $T(x,y)$ is represented by a PSD function means that the total system error will also be derived in terms of a PSD function. Integrating the error PSD according to Eq. (2.12) yields the mean square and, in turn, the rms value of the error. For several reasons, especially when dealing with noise inputs, it is advantageous to derive the expression for the autocorrelation function of the error and then to apply Eq. (2.10) to obtain the

the error PSD. If T' is the actual radiance of the ground scene after delay, as in Figure 3.2, it follows that the autocorrelation function of the error, $A_\varepsilon$, can be expressed by

$$\begin{aligned} A_\varepsilon &= E\{(T'-T_4)_+ (T'-T_4)\} \\ &= E\{T'_+T'\} + E\{T_{4+}T_4\} - E\{T'_+T_4\} - E\{T'T_{4+}\} \\ &= A_{T'}+A_{T_4} - C_{T'_+T_4} - C_{T'T_{4+}} \end{aligned} \tag{3.4}$$

Taking the Fourier transform of Eq. (3.4) leads to

$$P_\varepsilon = P_{T'} + P_{T_4} - P_{T'_+T_4} - P_{T'T_{4+}} \tag{3.5}$$

The input/output relationships of Section 2 are now used to evaluate the various terms in Eq. (3.4). It follows directly from Eq. (2.13) and Figure 3.2 that

$$A_{T'}(x,y) = A_T(x,y)*d(x)*d(-x) \tag{3.6}$$

where $d(x)$ is the impulse response function of the delay and $A_T(x,y)$ is the target radiance autocorrelation function. Taking the Fourier transform of Eq. (3.6) yields, from Eqs. (2.10) and (2.16),

$$P_{T'}(k_x,k_y) = |D(k_x)|^2 P_T(k_x,k_y) \tag{3.7}$$

where $D(k_x)$ is the transfer function of the delay and $P_T(k_x,k_y)$ is the input radiance PSD function. It is well known (see Section 4.10) that

$$|D(k_x)|^2 = 1$$

so that

$$P_{T'}(k_x,k_y) = P_T(k_x,k_y) \tag{3.8}$$

The evaluation of $A_{T_4}(x,y)$ is in principle identical to the evaluation of $A_{T'}(x,y)$ but more complicated. From Eq. (2.13) and Figure 3.2 it follows that

$$A_{T_4}(x,y) = [E\{T_3(\tilde{x},\tilde{y})_+T_3(\tilde{x},\tilde{y})\} + A_q(x)]*h_4(x,y)*h_4(-x,-y) \tag{3.9}$$

where $E\{T_3(\tilde{x},\tilde{y})_+T_3(\tilde{x},\tilde{y})\}$ is the autocorrelation function of the doubly sampled quantity $T_3(x,y)$, $A_q(x)$ is the autocorrelation function of the quantization noise and $h_4(x,y)$ is the impulse response function of the reconstruction filter. The effect of the x-sampler on $E\{T_3(x,\tilde{y})_+T_3(x,\tilde{y})\}$ is represented by (see Eq. (2.20))

$$E\{T_3(\tilde{x},\tilde{y})_+T_3(\tilde{x},\tilde{y})\} = \sum_{n=-\infty}^{\infty} \delta(x/x_i-n)E\{T_3(x,\tilde{y})_+T_3(x,\tilde{y})\} \tag{3.10}$$

Applying Eq. (2.13) to Figure 3.2 leads to

$$E\{T_3(x,\tilde{y})_+T_3(x,\tilde{y})\} = [E\{T_2(x,\tilde{y})_+T_2(x,\tilde{y})\} + A_d(x)]*h_3(x)*h_3(-x) \tag{3.11}$$

where $A_d(x)$ is the autocorrelation function of the detector and preamplifier noise. Similarly,

$$E\{T_2(x,\tilde{y})_+T_2(x,\tilde{y})\} = E\{T_1(x,\tilde{y})_+T_1(x,\tilde{y})\}*h_2(x)*h_2(-x) \tag{3.12}$$

$$E\{T_1(x,\tilde{y})_+T_1(x,\tilde{y})\} = \sum_{m=-\infty}^{\infty} \delta(y/y_i-m)A_{T_1}(x,y) \tag{3.13}$$

and

$$A_{T_1}(x,y) = A_T(x,y)*h_1(x,y)*h_1(-x,-y) \tag{3.14}$$

Substituting the results of Eqs. (3.10) through (3.14) into Eq. (3.9) gives

$$A_{T_4}(x,y) = h_4(x,y)*h_4(-x,-y)*\Bigg\{\sum_{n=-\infty}^{\infty} \delta(x/x_i-n)\,[h_2(x)*h_2(-x)*$$

$$\sum_{m=-\infty}^{\infty} \delta(y/y_i-m)A_T(x,y)*h_1(x,y)*h_1(-x,-y) + A_d(x)]*h_3(x)*h_3(-x)$$

$$+ A_q(x)\Bigg\} \tag{3.15}$$

Taking the Fourier transform of Eq. (3.15) leads to the PSD function of the output signal of the scanning system. Although composed of many more terms, the result is basically the result of Eq. (2.26). Thus,

$$P_{T_4}(k_x,k_y)=\left|H_4(k_x,k_y)\right|^2\sum_{n=-\infty}^{\infty}\sum_{m=-\infty}^{\infty}\left|H_1(k_x-\frac{n}{x_i},k_y-\frac{m}{y_i})H_2(k_x-\frac{n}{x_i})H_3(k_x-\frac{n}{x_i})\right|^2$$

$$\times P_T(k_x-\frac{n}{x_i},k_y-\frac{m}{x_i})$$

$$+\left|H_4(k_x,k_y)\right|^2\sum_{n=-\infty}^{\infty}\left|H_3(k_x-\frac{n}{x_i})\right|^2 P_d(k_x-\frac{n}{x_i})$$

$$+\left|H_4(k_x,k_y)\right|^2 P_q(k_x) \qquad (3.16)$$

where $P_d(k_x)$ and $P_q(k_x)$ are respectively the detector-preamplifier noise PSD and quantization noise PSD. The next step is to compute the crosscorrelation terms $C_{T',+T_4}$ in Eq. (3.4). The procedure is similar to that used to derive Eq. (3.16) but the input/output relationships are different. To clarify the procedure, Figure 3.2 will be cut at the comparator to indicate the direct link between $T_4(x,y)$ and $T'(x,y)$; see Figure 3.4.

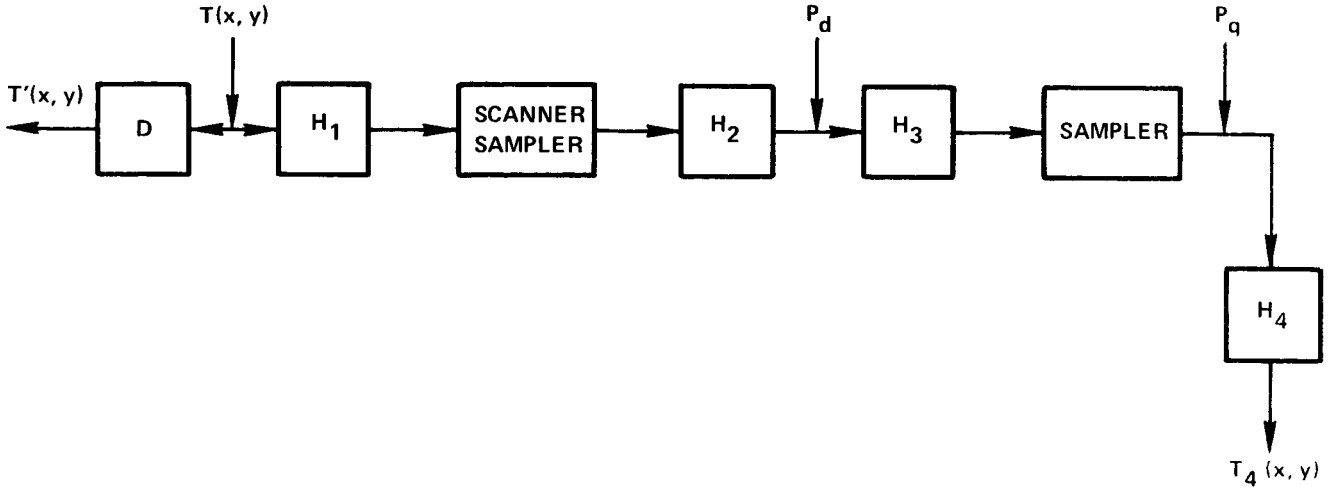


FIGURE 3.4

From Figure 3.4 and Eq. (2.14) it follows that

$$C_{T'+T_4}(x,y)=[E\{T'(x,y)+T_3(\tilde{x},\tilde{y})\}+C_{T'+q}(x)]*h_4(-x,-y) \qquad (3.17)$$

where $C_{T'+q}(x)$ is the crosscorrelation function of $T'(x,y)$ and the quantizing noise. If it is assumed that signal and noise are not correlated, then Eq. (3.17) becomes

$$C_{T'+T_4}(x,y)=E\{T'(x,y)+T_3(\tilde{x},\tilde{y})\}*h_4(-x,-y) \qquad (3.18)$$

From Eq. (2.21) it follows that

$$E\{T'(x,y)_{+}T_3(\tilde{x},\tilde{y})\}=E\{T'(x,y)_{+}T_3(x,\tilde{y})\} \tag{3.19}$$

It will now be assumed at the outset that detector-preamplifier noise is not correlated with the signal; then Eq. (2.14) gives

$$E\{T'(x,y)_{+}T_3(x,\tilde{y})\}=E\{T'(x,y)_{+}T_2(x,\tilde{y})\}*h_3(-x) \tag{3.20}$$

Next, from Eq. (2.14),

$$E\{T'(x,y)_{+}T_2(x,\tilde{y})\}=E\{T'(x,y)_{+}T_1(x,\tilde{y})\}*h_2(-x) \tag{3.21}$$

and, using Eq. (2.21),

$$E\{T'(x,y)_{+}T_1(x,\tilde{y})\}=E\{T'(x,y)_{+}T_1(x,y)\} \tag{3.22}$$

Continuing through the aperture,

$$E\{T'(x,y)_{+}T_1(x,y)\}=E\{T'(x,y)_{+}T(x,y)\}*h_1(-x,-y) \tag{3.23}$$

and, finally, from Eq. (2.15),

$$E\{T'(x,y)_{+}T(x,y)\}=A_T(x,y)*d(x) \tag{3.24}$$

Combining Eqs. (3.19) through (3.24) with Eq. (3.18) leads to

$$C_{T'_{+}T_4}=A_T*d(x)*h_1(-x,-y)*h_2(-x)*h_3(-x)*h_4(-x,-y) \tag{3.25}$$

Taking the Fourier transform of Eq. (3.25) gives a result similar to Eq. (2.17); thus,

$$P_{T'_{+}T_4}=A_T D(k_x)\bar{H}_1(k_x,k_y)\bar{H}_2(k_x)\bar{H}_3(k_x)\bar{H}_4(k_x,k_y) \tag{3.26}$$

Introducing a transfer function for an "advance" circuit, $A(k_x)$, it is noted that

$$\bar{A}(k_x) = D(k_x) \tag{3.27}$$

so that

$$P_{T'_+T_4} = P_T \bar{A}(k_x) \bar{H}_1(k_x,k_y) \bar{H}_2(k_x) \bar{H}_3(k_x) \bar{H}_4(k_x,k_y) \tag{3.28}$$

In a similar fashion, it can be shown that

$$P_{T'T_{4+}} = P_T A(k_x) H_1(k_x,k_y) H_2(k_x) H_3(k_x) H_4(k_x,k_y) \tag{3.29}$$

Substituting Eqs. (3.29), (3.28), (3.16) and (3.8) into Eq. (3.5) gives the PSD function of the error, $P_\varepsilon$, in the form

$$P_\varepsilon(k_x,k_y) = P_T(k_x,k_y)$$

$$+\left|H_4(k_x,k_y)\right|^2 \sum_{n=-\infty}^{\infty} \sum_{m=-\infty}^{\infty} \left|H_1(k_x - \frac{n}{y_i}, k_y - \frac{m}{y_i}) H_2(k_x - \frac{n}{x_i}) H_3(k_x - \frac{n}{x_i})\right|^2$$

$$\times P_T(k_x - \frac{n}{x_i}, k_y - \frac{m}{y_i})$$

$$-2\mathrm{Re}\left[P_T(k_x,k_y) A(k_x) H_1(k_x,k_y) H_2(k_x) H_3(k_x) H_4(k_x,k_y)\right]$$

$$+\left|H_4(k_x,k_y)\right|^2 \sum_{n=-\infty}^{\infty} \left|H_3(k_x - \frac{n}{x_i})\right|^2 P_d(k_x - \frac{n}{x_i})$$

$$+\left|H_4(k_x,k_y)\right|^2 P_q(k_x) \tag{3.30}$$

where Re[ ] indicates the real part if the quantity.
The first three terms of Eq. (3.30) can be combined so that $P_\varepsilon(k_x,k_y)$ becomes

$$P_\varepsilon = P_T(k_x,k_y)\left|H_1H_2H_3H_4A - 1\right|^2$$

$$+\left|H_4(k_x,k_y)\right|^2 \sum_{\substack{n=-\infty \\ n,m\neq 0}}^{\infty}\sum_{m=-\infty}^{\infty}\left|H_1(k_x - \frac{n}{x_i}, k_y - \frac{m}{y_i})H_2(k_x - \frac{n}{x_i})H_3(k_x - \frac{n}{x_i})\right|^2$$

$$\times P_T(k_x - \frac{n}{x_i},\ k_y - \frac{m}{y_i})$$

$$+\left|H_4(k_x,k_y)\right|^2 \sum_{n=-\infty}^{\infty}\left|H_3(k_x - \frac{n}{x_i})\right|^2 P_d(k_x - \frac{n}{x_i})$$

$$+\left|H_4(k_x,k_y)\right|^2 P_q(k_x) \qquad (3.31)$$

Eq. (3.31) conveniently breaks out into four distinct terms. The first two are termed the fidelity PSD terms, one being the classical fidelity term and the other the contribution due to sampling (also known as the aliasing terms). The third and fourth terms are the contributions to the error due to detector-preamplifier noise and quantizing noise. The mean square error, $\varepsilon^2$, from Eq. (2.12), is

$$\varepsilon^2 = \iint_{-\infty}^{\infty} P_\varepsilon(k_x,k_y)\,dk_x dk_y$$

$$= \varepsilon_f^{\,2} + \varepsilon_d^{\,2} + \varepsilon_q^{\,2} \qquad (3.32)$$

where the fidelity error is

$$\varepsilon_f^2 = \iint_{-\infty}^{\infty} P_T(k_x,k_y) \left| H_1H_2H_3H_4A - 1 \right|^2 dk_x dk_y$$

$$+ \iint_{-\infty}^{\infty} \left| H_4(k_x,k_y) \right|^2 \sum_{\substack{n=-\infty \\ n,m\neq 0}}^{\infty} \sum_{m=-\infty}^{\infty} \left| H_1(k_x - \frac{n}{x_i}, k_y - \frac{m}{y_i}) H_2(k_x - \frac{n}{x_i}) H_3(k_x - \frac{n}{x_i}) \right.$$

$$\left. \times H_4(k_x - \frac{n}{x_i}, k_y - \frac{m}{y_i}) \right|^2 P_T(k_x - \frac{n}{x_i}, k_y - \frac{m}{y_i}) \quad dk_x dk_y \tag{3.33}$$

the detector-preamplifier noise error is

$$\varepsilon_d^2 = \iint_{-\infty}^{\infty} \left\{ \left| H_4(k_x,k_y) \right|^2 \sum_{n=-\infty}^{\infty} \left| H_3(k_x - \frac{n}{x_i}) \right|^2 P_d(k_x - \frac{n}{x_i}) \right\} dk_x dk_y \tag{3.34}$$

and the quantizing noise error is

$$\varepsilon_q^2 = \iint_{-\infty}^{\infty} \left| H_4(k_x,k_y) \right|^2 P_q(k_x) dk_x dk_y \tag{3.35}$$

The rms error is formed from Eq. (3.32):

$$\varepsilon = (\varepsilon_f^2 + \varepsilon_d^2 + \varepsilon_q^2)^{1/2} \tag{3.36}$$

The next step is to normalize the rms error with respect to the mean value of ground radiance.

## 3.4 Mean Target Radiance

A value for mean target radiance, $\bar{T}$, is now derived so that it may be used as a normalizing factor for the rms error. The equation for variance, Eq. (3.2), may be expanded in the form

$$\sigma_T^2 = E\{(T(x,y)-\bar{T})^2\} = E\{T^2(x,y)\} - 2E\{T(x,y)\bar{T}\} + E\{\bar{T}^2\} \tag{3.37}$$

$$= 1$$

where $\bar{T}$ is the mean value. Clearly,

$$E\{T^2(x,y)\} = \overline{T^2} \tag{3.38}$$

where $\overline{T^2}$ is the mean square value of radiance. Also,

$$E\{T(x,y)\bar{T}\} = \bar{T}E\{T(x,y)\} = \bar{T}^2 \tag{3.39}$$

where $\bar{T}^2$ is the square of the mean value of radiance. Finally,

$$E\{\bar{T}^2\} = \bar{T}^2 \tag{3.40}$$

since $\bar{T}$ is a constant. Substituting Eqs. (3.40), (3.39) and (3.38) into (3.37) yields

$$\overline{T^2} - \bar{T}^2 = 1 \tag{3.41}$$

It is now assumed that the range of expected radiance values will be equal to the mean radiance; that is,

$$\Delta T = \bar{T} \tag{3.42}$$

Furthermore, it is assumed that all values are equally probable. That is, if f(T) is the probability density function for T(x,y), then

$$\left.\begin{aligned} f(T) &= \frac{1}{\bar{T}} \quad (\text{const.}),\ \bar{T}-\bar{T}/2 \leq T(x,y) \leq T+\bar{T}/2 \\ \text{and} \\ f(T) &= 0, \text{ all other values of } T \end{aligned}\right\} \tag{3.43}$$

Note that the required condition of probability density functions is satisfied:

$$\int_{-\infty}^{\infty} f(T)\,dT = \frac{1}{\bar{T}} \int_{\bar{T}/2}^{3\bar{T}/2} dT \equiv 1$$

The mean square value of radiance, $\overline{T^2}$, can be computed from

$$\overline{T^2} = \int_{-\infty}^{\infty} f(T)T^2 dT = \frac{1}{\bar{T}} \int_{\bar{T}/2}^{3\bar{T}/2} T^2 dT = \bar{T}^2\left(\frac{26}{24}\right) \tag{3.44}$$

Combining (3.44) and (3.41)

$$\left.\begin{aligned} \bar{T}^2 &= 12 \\ \text{or} \\ \bar{T} &= \sqrt{12} \end{aligned}\right\} \tag{3.45}$$

This value of mean radiance can be used to normalize the rms error; thus, dividing through Eq. (3.36) by $\bar{T}$ gives

$$\bar{\varepsilon} = \left(\bar{\varepsilon}_f^{\,2} + \bar{\varepsilon}_d^{\,2} + \bar{\varepsilon}_q^{\,2}\right)^{1/2} \tag{3.46}$$

where $\bar{\varepsilon}$ is the total normalized rms system error; thus,

$$\bar{\varepsilon} = \varepsilon/\bar{T} \tag{3.47}$$

$$\bar{\varepsilon}_f = \varepsilon_f/\bar{T} \tag{3.48}$$

$$\bar{\varepsilon}_d = \varepsilon_d/\bar{T} \tag{3.49}$$

and

$$\bar{\varepsilon}_q = \varepsilon_q/\bar{T} \tag{3.50}$$

## 4.0 DETAILS OF SYSTEM PARAMETERS FOR THE S-192 SCANNER

### 4.1 Signal-to-noise Ratio of the Detector

The detector signal-to-noise ratio must be established so that it may be used to scale the detector noise PSD function described in Section 4.4. The signal-to-noise ratio is obtained directly from projected or measured NE$\Delta\rho$ values of the particular channels. Due to the stochastic representations of noise and signal, NE$\Delta\rho$ will be defined as the ratio of rms noise, $\bar{n}$, to rms signal, $(\overline{T^2})^{1/2}$, and, therefore is a direct inverse of a signal-to-noise ratio. From this definition,

$$\left(\frac{\bar{n}^2}{\overline{T^2}}\right)^{1/2} = NE\Delta\rho$$

and it follows from Eqs. (3.41) and (3.45) that

$$\bar{n} = (\sqrt{13}) \, NE\Delta\rho \tag{4.1}$$

where $\bar{n}$ is found from

$$\bar{n}^2 = 2a^2 \int_0^\infty P_d(f) \left| H_3(f) \right|^2 df \tag{4.2}$$

The constant $a^2$ in Eq. (4.2) is the scale factor to be determined. Combining Eqs. (4.1) and (4.2), lead to

$$a = \frac{(\sqrt{13}) \, NE\Delta\rho}{\left[2 \int_0^\infty P_d(f) \left| H_3(f) \right|^2 df\right]^{1/2}} \tag{4.3}$$

Projected values of $NE\Delta\rho$ for the S-192 Multispectral Scanner can be found in Reference 4. As shown in Section 4.4, $a^2$ is used as a scale factor for the detector-preamplifier noise PSD. This is how $NE\Delta\rho$ is incorporated directly into the overall rms system error.

## 4.2 Detector Parameters

Photoconductive Time Constant: The frequency at which the detector responsivity begins to roll off is designated $f_r$. It is related to the photoconductive time constant, $\tau_{pc}$, through

$$\tau_{pc} = \frac{1}{2\pi f_r} \tag{4.4}$$

(See Figure 4.1 for a representation of detector response.) Actual S-192 detectors have values of $\tau_{pc}$ in the neighborhood of 40$\mu$ seconds.

Detective Time Constant: The frequency at which generation - recombination noise intersects the Johnson noise level is refered to as $f_d$. The detective time constant, $\tau_d$, is related to $f_d$ through

$$\tau_d = \frac{1}{2\pi f_d} \tag{4.5}$$

Values of $\tau_d$ of 1$\mu$ second are claimed for the S-192 detectors.

## 4.3 Required System Bandwidth

The system bandwidth is based on the sampling rate (Samples/IFOV*) and orbital parameters of the Skylab spacecraft.

---

*IFOV - Instantaneous Field of View

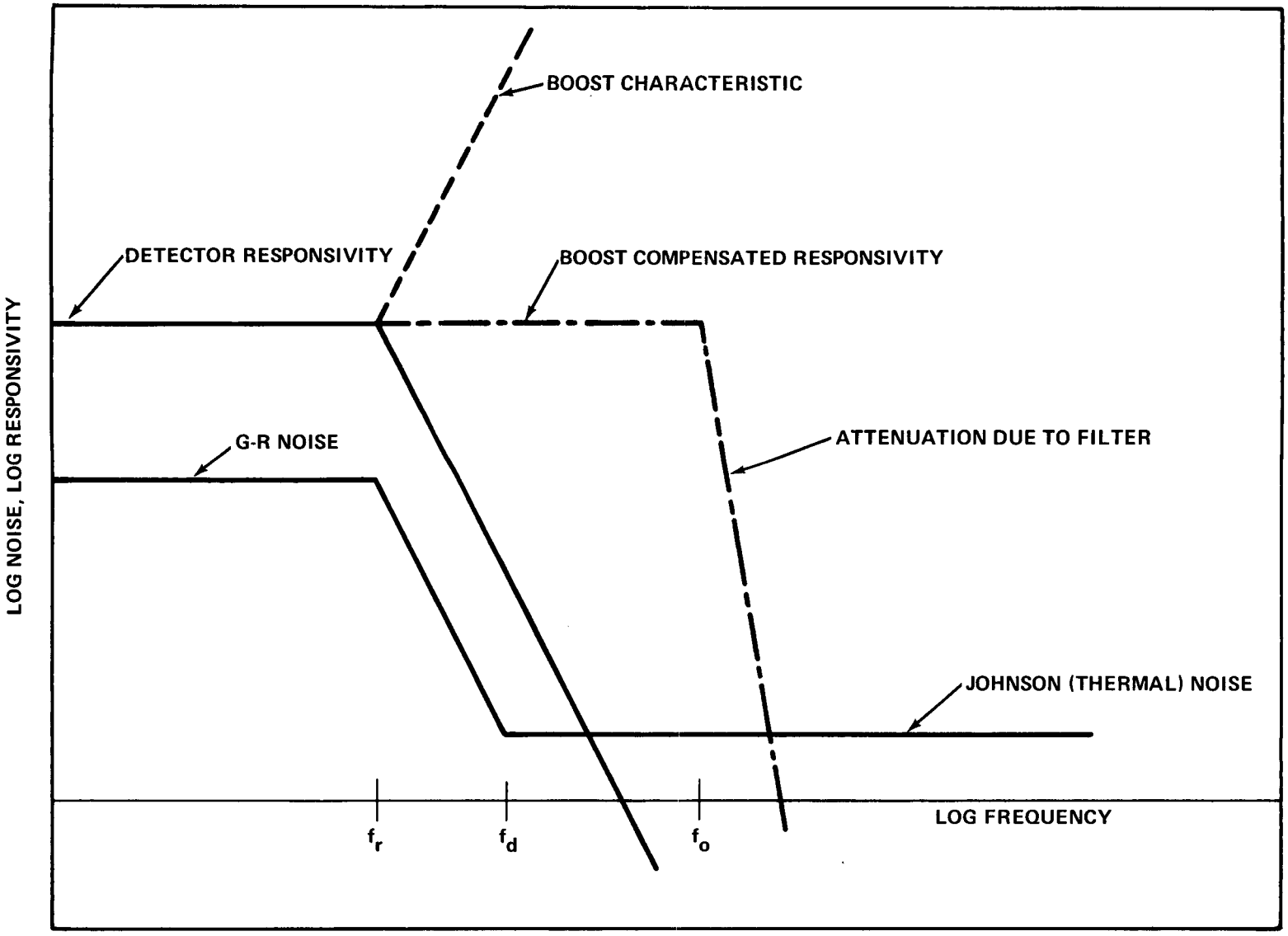
BOOST CHARACTERISTIC
DETECTOR RESPONSIVITY
BOOST COMPENSATED RESPONSIVITY
G-R NOISE
ATTENUATION DUE TO FILTER
JOHNSON (THERMAL) NOISE
LOG NOISE, LOG RESPONSIVITY
LOG FREQUENCY
$f_r$
$f_d$
$f_o$

FIGURE 4.1

It is derived by taking half the information bandwidth of the system. For S-192, taking 1 sample/IFOV, it can be shown that the required system electrical bandwidth, $f_0$, is

$$f_0 = 167 \text{ KHz} \tag{4.6}$$

4.4 Detector - Preamplifier Noise Bandwidth

The detector-preamplifier noise PSD, $P_d(f)$, can be represented by [3,4]

$$P_d(f) = a^2\left[\frac{1 + (f/f_d)^2}{1 + (f/f_r)^2} + b\left(\frac{f_r}{f_d}\right)^2\right] \tag{4.7}$$

where f is frequency in Hertz, a is the constant defined in Eq. (4.3) and b is a constant involving a number of factors such as temperature of the detectors, temperature of the transistors, detector resistance, etc. [4] The relationship between the temporal frequency f, the x-spatial frequency, $k_x$, and the scanning rate along the x direction, v, is

$$f = v\, k_x \tag{4.8}$$

Thus, Eq. (4.7) can be written

$$P_d(v\, k_x) = a^2\left[\frac{1 + (k_x/k_{xd})^2}{1 + (k_x/k_{xr})^2} + b\left(\frac{k_{xr}}{k_{xd}}\right)^2\right] \tag{4.9}$$

where $k_{xr} = f_r/v$

and $k_{xd} = f_d/v$

Actually, one more operation is required on Eq. (4.9) before it can be substituted into Eq. (3.34). The represention of Eq. (4.9) is based on the one dimensional character of the detector-preamp noise and is really suited for evaluation by a one dimensional integration in $k_x$. Therefore, Eq. (4.9) should be normalized by a factor

$$\int_{-\infty}^{\infty} |H_4(k_x,k_y)|^2 dk_y.$$

## 4.5 Quantization Noise PSD

The mean square error due to quantizing is given by [13]

$$\varepsilon_q^2 = \frac{1}{12}\left(\frac{1}{2^{2n}}\right)\Delta T^2 \tag{4.10}$$

where n is the number of bits assigned to each quantizing level and $\Delta T$ is, as defined in Section 3.4, the expected range of radiance values. The normalized mean square value of quantizing error is

$$\bar{\varepsilon}_q^2 = \frac{1}{12}\left(\frac{1}{2^{2n}}\right)\left(\frac{\Delta T}{\bar{T}}\right)^2$$

or, recalling Eq. (3.42),

$$\bar{\varepsilon}_q^2 = \frac{1}{12}\left(\frac{1}{2^{2n}}\right) \tag{4.11}$$

Since $\bar{\varepsilon}_q$ can be computed directly, there is no necessity to construct a PSD function, $P_q$, for quantizing noise. Actually, $P_q$ simply served as a formalism in the derivation of Eq. (3.35).

4.6 Aperture Transfer Function

The system aperture transfer function is defined as the Fourier transform of a rectangular scanning aperture divided by the area of the aperture. The impulse response function of such an aperture is

$$h_1(x,y) = \begin{cases} 1/x_d y_d, & |x| \leq \frac{x_d}{2}, |y| \leq \frac{y_d}{2} \\ 0, \text{ all other } x \text{ and } y \end{cases}$$

The corresponding transfer function is

$$H_1(k_x,k_y) = \frac{\sin(\pi x_d k_x)\sin(\pi y_d k_y)}{x_d y_d \, k_x k_y \pi^2} \tag{4.12}$$

The actual S-192 IFOV is $1.82 \times 10^{-4}$ radians which, using Skylab orbital parameters, projects a 260'x260' rectangle on the ground. Thus, $x_d=y_d=260$ ft.

## 4.7 Detector Transfer Function

The detector is assumed to have a transfer function of the form

$$H_2(f) = \frac{1}{1+j\ f/f_r} \tag{4.14}$$

where $j = \sqrt{-1}$. Using Eq. (4.8), Eq. (4.14) can be written

$$H_2(v\ k_x) = \frac{1}{1+j(k_x/k_{xr})} \tag{4.15}$$

For the S-192 system, $f_r \cong$ 4KHz meaning that detector response begins rolling off around 4KHz.

## 4.8 Detector Electronics Transfer Function

Detector electronics encompasses the preamplifier, boost circuit and filter. Each component will be described separately.

Preamplifier: The preamplifier transfer function is described by

$$H_p(f) = \frac{1}{1+j\ f/f_p} \tag{4.16}$$

where, for the S-192, $f_p$ = 2.0 MHz.

Boost Circuit: As stated in Section 4.7, the detector response begins rolling off at 4 KHz. Eq. (4.6), on the other hand, states that the required system bandwidth $f_0$ is 167 KHz. A boost network is therefore introduced to enhance the detector response over the required bandwidth. The transfer function for the boost network takes the form

$$H_B(f) = \frac{f_b}{f_r}\left(\frac{jf + f_r}{jf + f_b}\right) \tag{4.17}$$

For the S-192 system, $f_b$ = 260 KHz.

System Filters: The S-192 has a 2 pole Butterworth filter rolling off at the system bandwidth and has, in addition 3 poles of RC filtering; there is a double pole at $f_1$ = 600 KHz and a single pole at $f_2$ = 450 KHz. Thus, the filter transfer function takes the form

$$H_F(f) = \frac{1}{[.707+j(f/f_0+.707)][.707+j(f/f_0-.707)][j\ f/f_1+1]^2[j\ f/f_2+1]} \tag{4.18}$$

The simulation has been kept flexible enough to incorporate any kind of filtering. Combining Eqs. (4.16), (4.17) and (4.18) leads to the transfer function of the detector electronics;

$$H_3(f) = H_p(f)H_B(f)H_F(f) \tag{4.19}$$

## 4.9 Reconstruction Filter

Ideal reconstruction is assumed; that is, the impulse response function of the reconstruction filter is

$$h_4(x,y) = \frac{\sin \pi x/x_i \ \sin \pi y/y_i}{\pi^2 xy}$$

where it is recalled that $x_i$ and $y_i$ are the x and y distances between samples. The corresponding transfer function is

$$H_4(k_x,k_y) = \begin{cases} 1, & k_x \leq \left|\frac{1}{2x_i}\right|, k_y \leq \left|\frac{1}{2y_i}\right| \\ 0, & k_x > \left|\frac{1}{2x_i}\right|, k_y > \left|\frac{1}{2y_i}\right| \end{cases} \tag{4.20}$$

## 4.10 Delay Transfer Function

The delay takes the standard form

$$D(f) = e^{-2\pi j f t_d} \tag{4.21}$$

or, from Eq. (4.8)

$$D(vk_x) = e^{-2\pi j k_x S_d} \tag{4.22}$$

where $t_d$ is the delay in the upper loop of Figure (3.2) and $S_d = vt_d$ is an equivalent distance delay. Note that

$$|D|^2 = 1.$$

## 4.11 Parameters Available for Variation

The system parameters that were varied in the simulation are listed below.

Aperture and Scale Distance ($x_T/x_d$): The ratio of $x_T/x_d$ represents the resolution capability of the system in relation to a particular ground scene. When $x_T/x_d = 1$, the ground radiance autocorrelation function half amplitude point is equal to the IFOV. As the ratio $x_T/x_d$ increases beyond unity, the relative resolution capability of the instrument improves and the rms error should decrease. For ground scenes with high information content, that is, $x_T/x_d < 1$, the error should be greater.

Scanning/Sampling: It is not generally true that increased sampling continues to improve system accuracy. Even in noisless systems there are two factors limiting increased accuracy through increased sampling. First, a theoretical factor, the Shannon sampling theorem [11], states that a band limited signal with a

finite upper frequency limit of F Hz. can be completely specified by sampling at instants of time separated by 1/2F. Although the radiance signal represented by Eq. (3.3) is not bandlimited, the effect of the aperture function and subsequent filtering (before sampling) is to produce an almost bandlimited signal with little frequency content above the bandwidth of the S-192 system. Hence little improvement in system accuracy should be expected by sampling more than twice per IFOV. Second, there is the practical consideration of the sampling method in the S-192 scanner. With a fixed scan rate v, a particular IFOV is always sampled once in the y- direction while increased sampling rates mean that only the number of cross track, or x, samples increases. Thus, additional information on the y-dependent portion of the signal is not gained, and this places another limit on improvement through sampling. These two reasons do not, however, represent the main argument against unlimited increase in sampling rates. The utilization of an increased number of samples/IFOV requires that the system bandwidth be proportionately increased. This requirement leads to additional boosting of the detector response. Boosting beyond the detector frequency $f_d$ leads to a disproportional increase in noise relative to signal. Thus it is clear that an optimum bandwidth and a corresponding optimum sampling rate will exist.

## 5.0 RESULTS OF THE SIMULATION FOR THE S-192 SCANNER

### 5.1 Simulation Output

The simulation results of the rms error analysis include:

- $\bar{\varepsilon}_f$ - normalized rms fidelity error (Eqs. (3.33) and (3.48)):
- $\bar{\varepsilon}_d$ - normalized rms detector-preamp noise error (Eqs. (3.34) and (3.49)):
- $\bar{\varepsilon}_q$ - normalized rms quantizing noise error (Eqs. (3.35) and (3.50)):
- $\bar{\varepsilon}$ - total normalized rms system error (Eqs. (3.36) and (3.47)).

For the actual calculation of $\bar{\varepsilon}_q$, Eq. (4.11) is used. This quantity remains constant for all cases. In the S-192 system, the number of bits assigned to each quantizing level is n=8; thus,

$$\bar{\varepsilon}_q = .001128$$

Aside from the two major parameter variations discussed in Section 4.11, the results presented are also representative of the noise properties of typical channels. Projected [4] maximum and minimum NE$\Delta\rho$ channels were selected and a nominal (NE$\Delta\rho$ = 1%) channel was constructed; their properties are listed below:

| | $\tau_{pc}$ | $\tau_d$ | NE$\Delta\rho$ |
|---|---|---|---|
| Channel 1 | 44μsec | 1μsec | 3.0 % |
| Channel 7 | 40μsec | 1μsec | 0.57% |
| Nominal | 40μsec | 1μsec | 1.0 % |

## 5.2 Discussion of Results

Variation of Resolution Capability ($x_T/x_d$): Figure 5.1 illustrates the expected reduction in $\bar{\varepsilon}_f$ as $x_T/x_d$ increases and also indicates the effect of placing the delay in the lower loop.* The normalized rms fidelity error drops below 10% when $x_T/x_d = 2$ and one sample per IFOV is taken. Figure 5.2 illustrates the variation of total rms error for the three channels of interest. The effect of higher NE$\Delta\rho$ is apparent.

Effects of Sampling: Figure 5.3 shows the variation of $\bar{\varepsilon}_f$, $\bar{\varepsilon}_d$ and $\bar{\varepsilon}$ with sampling rate for channel 1 when $x_T/x_d$ is unity.** The fidelity error, $\bar{\varepsilon}_f$, drops steadily with increasing sampling rate until it approaches an asymptotic value of about 12.7% at 2 samples per IFOV. (This curve is the same for all channels as it is independent of noise.) The results of Figures 5.3, 5.4, and 5.5 reflect the fact that the system bandwidth is expanded proportionately to accommodate the higher sampling rates. As asserted in Section 4.11, the rms detector-preamp noise increases rapidly with increasing sampling rate and soon wipes out any improvement in fidelity error. Significantly, for Channel 1, the optimum sampling rate (minimum $\bar{\varepsilon}$) is less than one sample per IFOV. Figure 5.4 illustrates the effect of sampling rates on the projected minimum NE$\Delta\rho$ channel, channel 7. Here, the optimum sampling rate is about 1.8 samples per IFOV. The same information for the nominal channel, the one meeting the EIS noise specification (NE$\Delta\rho$ = 1%), is contained in Figure 5.5 and the optimum sampling

---

*All subsequent results include the delay.

**The case $x_T/x_d = 1$ is felt to be representative of the kind of ground scene the instrument might be reasonably expected to handle. This can be justified by noting Figure 5.1 which indicates that for values of $x_T/x_d$ less than unity, the fidelity error increases beyond an acceptable point (15%).

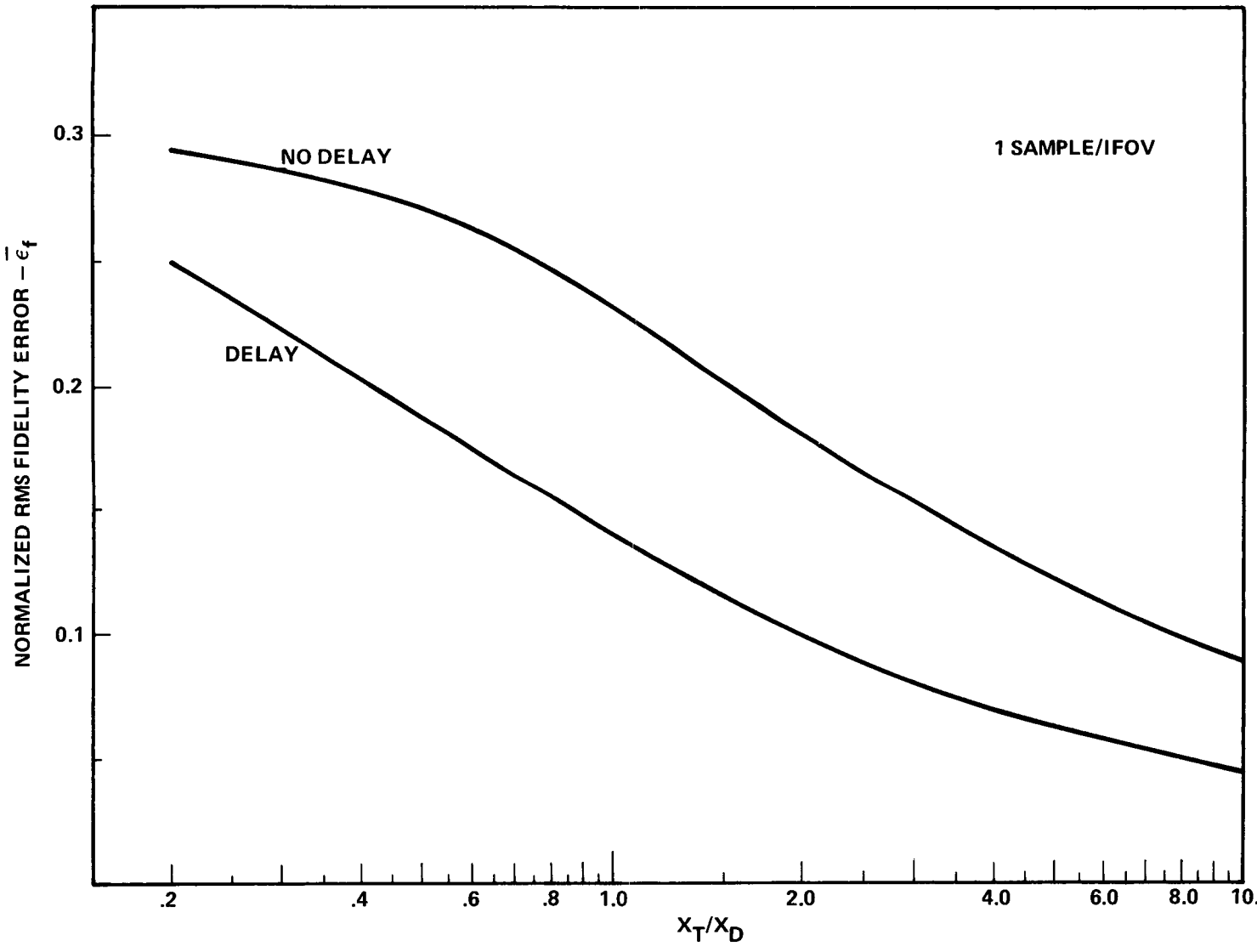


FIGURE 5.1 - RMS FIDELITY ERROR VS. VARYING GROUND DETAIL

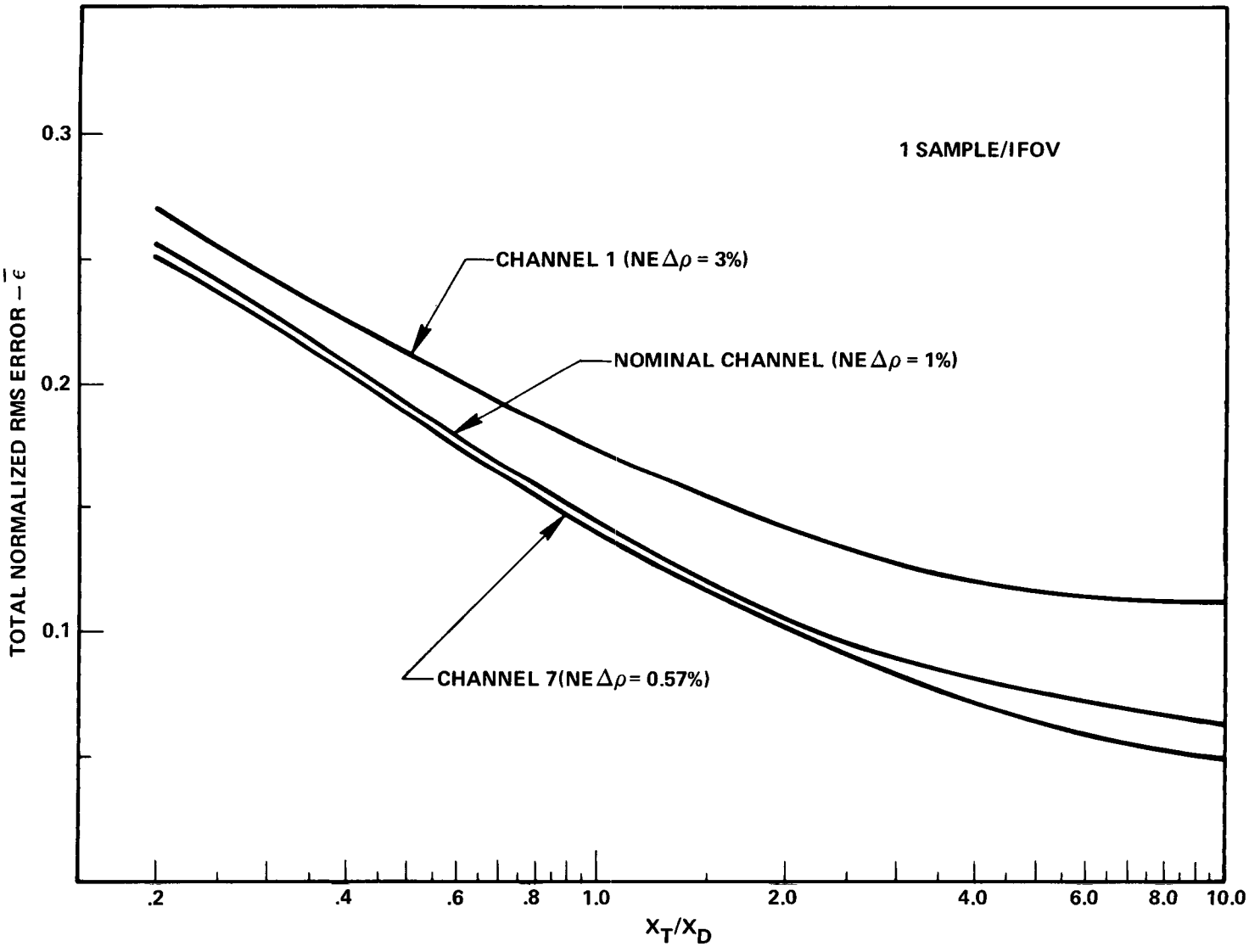


FIGURE 5.2 - RMS ERROR VS. VARYING GROUND DETAIL

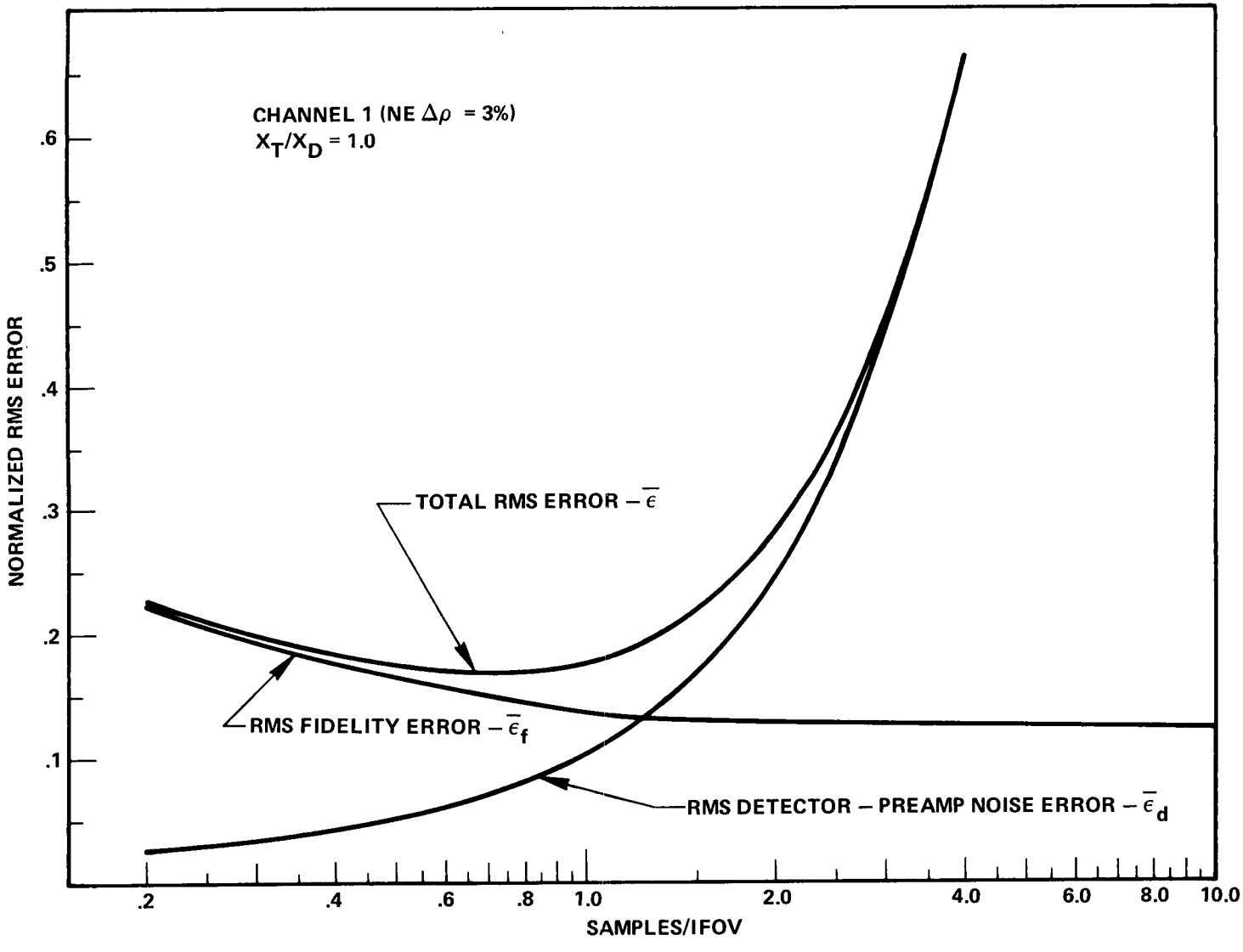


FIGURE 5.3 - RMS ERROR VS SAMPLING RATE

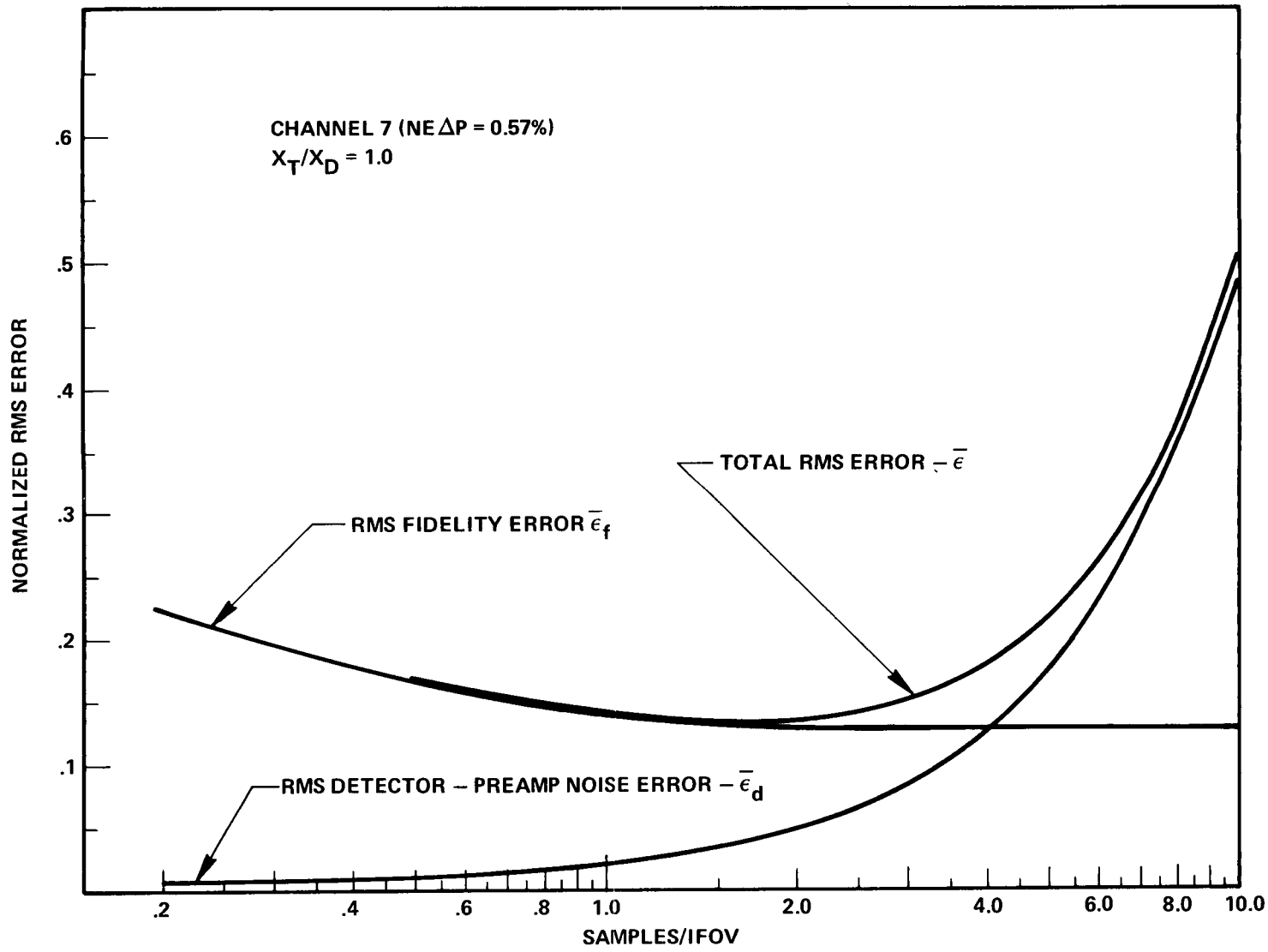


FIGURE 5.4 - RMS ERROR VS SAMPLING RATE

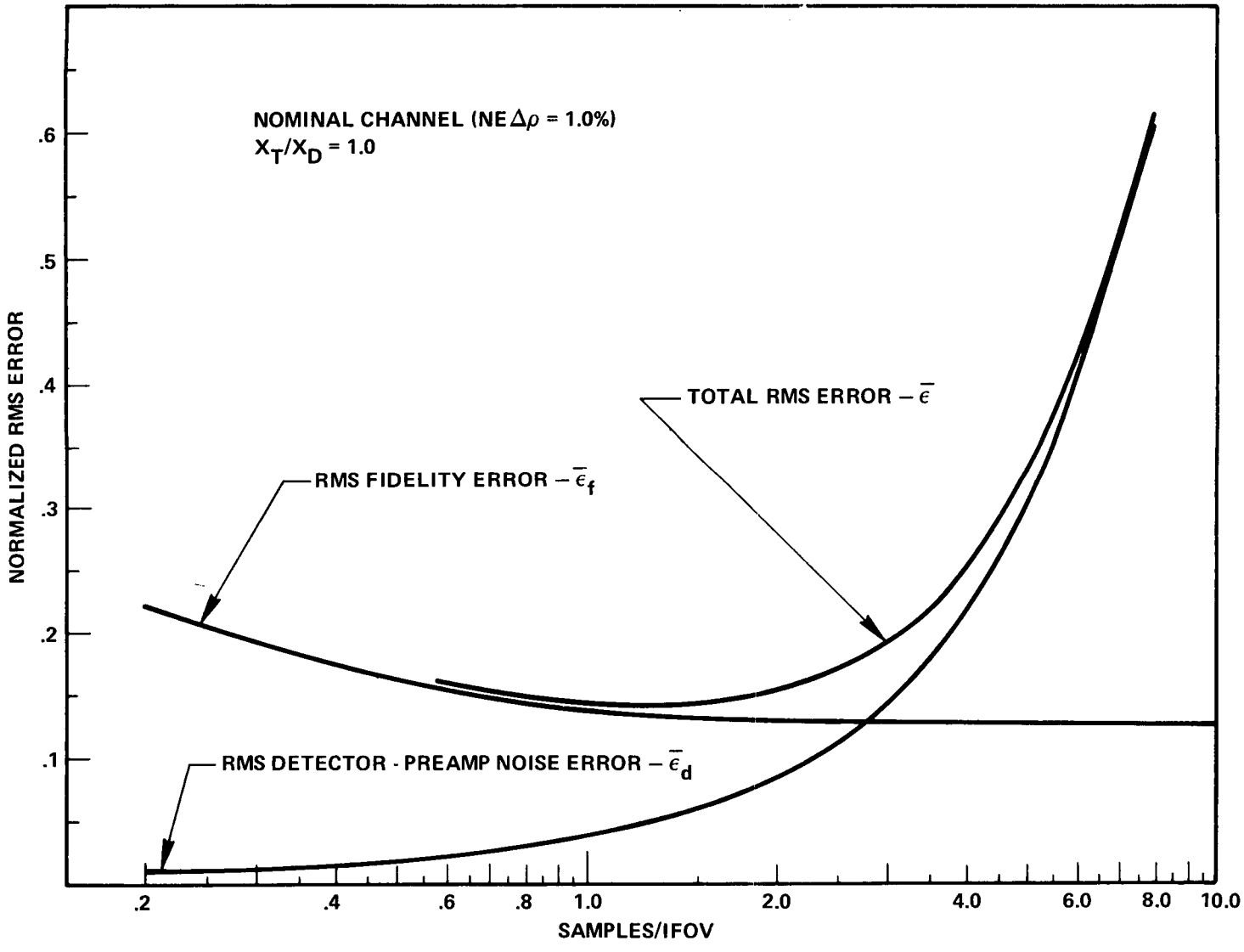


FIGURE 5.5 - RMS ERROR VS. SAMPLING RATE

rate is seen to be 1.3 samples per IFOV. Because the total rms system error has a shallow minimum, a sampling rate of 1.1 samples per IFOV is close to optimum.

Several runs were made where sampling rate was varied while system bandwidth was held constant at nominal value. The maximum improvement in $\bar{\varepsilon}_f$ for this procedure was under 0.5%. The original S-192 design had four "high" resolution channels (130' x 130') which were sampled at twice the rate of the "low" resolution channels (260' x 260'). Detector development problems led to replacement of the "high" resolution channels with "low" resolution channels [3] although the sampling rate in these bands was left unchanged to avoid impacting the timing and recording schemes. Thus eight of the channels are being sampled 2.2 times per IFOV although their bandwidth fits the one sample per IFOV value (167 KHz). As mentioned above, additional sampling without additional bandwidth adds nothing to system accuracy but does add unnecessarily to the bit rate.

Filtering: Filter variations, say 5 pole Butterworth instead of 2 pole Butterworth - 3 pole RC, do not significantly impact overall system error. Ground scene and aperture are the major contributors to fidelity error and changes in equivalent system bandwidth of about 10% will not greatly effect the final result.

## 6.0 CONCLUSIONS

The major conclusions of this study are:

1. The optimum sampling rate for a channel whose detector just meets noise specification is 1.3 samples per IFOV.

2. The present S-192 design sampling rate for five of the thirteen channels is 1.1 samples per IFOV. Because the total system error has a shallow minimum, the design sampling rate is close to optimum. This result is in opposition to the view held in some quarters that the S-192 system is digital data bandwidth limited.

3. Sampling the remaining eight channels at a rate of 2.2 samples per IFOV does not improve system performance.

4. The approach used in this paper to evaluate the performance of scanning systems provides an effective, workable tool for design and analysis.

Acknowledgements: Many helpful and informative discussions concerning this work were held with G. M. Anderson and S. Y. Lee. Miss Linda Hawkins did a first rate job in writing the programs for the simulation.

1022-RJR-mef

R. J. Ravera

Attachments

## References


1. "End Item Specification for Multispectral Scanner", MSC-TF-192-111, August 28, 1971.
2. Hudson, R. D., Infrared Systems Engineering, Wiley Interscience, 1969, pp. 266-271.
3. Anderson, G. M., and Ravera, R. J., "S-192 Multispectral Scanner Review", Bellcomm Memorandum for File, B71 06007, June 4, 1971.
4. Anderson, G. M., and Ravera, R. J., "S-192 Multispectral Scanner Performance Projections", Bellcomm Memorandum for File, B71 08023, August 18, 1971.
5. Goodman, J. W., Introduction to Fourier Optics, McGraw-Hill, 1969.
6. Lee, Y. W., Statistical Theory of Communication, Wiley, 1961, pp.204, 56-66, 331-332.
7. Cheng, G. C., and Ledley, R. S., "A Theory of Picture Digitization and Applications", Pictorial Pattern Recognition, Thompson Book Company, 1968.
8. Lee, S. Y., "Characterization and Mathematical Representation of Line Scanning Image Systems", Bellcomm TM-71-1031-2, May 25, 1971, p. 14.
9. Zachor, A. S., and Tretiak, O. J., Unpublished analysis accompanying Honeywell Radiation Center Customer Engineering Letter 71-CEL-41, March 18, 1971.
10. Papoulis, A., The Fourier Integral and its Applications, McGraw-Hill, 1962, pp. 269-282, 244, 273-275, 42-45.
11. Ragazzini, J. R., and Franklin, G. F., Sampled Data Control Systems, McGraw-Hill, 1958, pp. 255-287, 16.
12. Kuo, B. C., Analysis and Synthesis of Sampled Data Control Systems, Prentice Hall, 1963, pp. 397-410.
13. Bennet, W. R., Introduction to Signal Transmission, McGraw-Hill, 1970, p. 144.

# APPENDIX A

## Theorems on Sampled Functions

Several theorems on sampled functions which are used in the main portion of this report are proven here. Some of the theorems of Appendix A (and of Appendix B), in one form or another, appear elsewhere [8,10,11,12]. The reason for repeating them here is to present them in a more unified context.

The following lemmas, necessary in the proofs to follow, will be stated. Proofs may be found in Papoulis [10].

Lemma 1:

$$f(t)\delta(t-t_0) = f(t_0)\delta(t-t_0) \tag{A-1}$$

where $\delta(t)$ is the unit impulse (Dirac delta) function.

Lemma 2:

$$\delta(t-t_1)*\delta(t-t_2) = \int_{-\infty}^{\infty} \delta(\tau-t_1)\delta(t-\tau-t_2)d\tau$$

$$= \delta[t-(t_1+t_2)] \tag{A-2}$$

Lemma 3:

$$\delta(at-t_0) = \frac{1}{|a|}\delta(t-t_0/a) \tag{A-3}$$

Assuming stationary and ergodic functions, the one dimensional autocorrelation and crosscorrelation functions can be written

$$E\{x_+x\} = A_x(\zeta) = \lim_{T\to\infty} \frac{1}{2T} \int_{-T}^{T} x(t)x(t+\zeta)dt \tag{A-4}$$

$$E\{x_+y\} = C_{x_+y}(\zeta) = \lim_{T\to\infty} \frac{1}{2T} \int_{-T}^{T} x(t+\zeta)y(t)dt \qquad (A\text{-}5)$$

and

$$E\{xy_+\} = C_{xy_+}(\zeta) = \lim_{T\to\infty} \frac{1}{2T} \int_{-T}^{T} x(t)y(t+\zeta)dt \qquad (A\text{-}6)$$

Given a function $x(t)$ whose first derivative is piecewise continuous and whose amplitude is sampled at intervals of $t_i$; the sampled function, $x(\tilde{t})$, will be represented by

$$x(\tilde{t}) = \sum_{m=-\infty}^{\infty} x(t)\,\delta(t/t_i - m).$$

Theorem 1:

The crosscorrelation function of two sampled functions, $x(\tilde{t})$ and $y(\tilde{t})$,

where $$x(\tilde{t}) = \sum_{m=-\infty}^{\infty} x(t)\,\delta(t/t_i - m) \qquad (A\text{-}7)$$

and $$y(\tilde{t}) = \sum_{k=-\infty}^{\infty} y(t)\,\delta(t/t_i - k) \qquad (A\text{-}8)$$

may be represented by*

$$E\{x(\tilde{t})_+ y(\tilde{t})\} = \sum_{m=-\infty}^{\infty} C_{x_+y}(t)\,\delta(t/t_i - m) \qquad (A\text{-}9)$$

---

*The "expected value" representation of the autocorrelation and crosscorrelation functions is superior because it clearly shows which quantity is sampled and the independent variable involved in the sampling process.

Proof:

From (A-1) and (A-3), noting that $t_i > 0$, (A-7) and (A-8) can be written

$$\tilde{x}(t) = t_i \sum_{m=-\infty}^{\infty} x(mt_i)\,\delta(t-mt_i) \tag{A-10}$$

and

$$\tilde{y}(t) = t_i \sum_{k=-\infty}^{\infty} y(kt_i)\,\delta(t-kt_i) \tag{A-11}$$

Substituting (A-10) and (A-11) into (A-5) gives

$$E\{\tilde{x}(t)_+\, \tilde{y}(t)\} =$$

$$\lim_{T\to\infty} \frac{1}{2T}\, t_i^{\,2} \int_{-T}^{T} \left\{ \sum_{k=-\infty}^{\infty} y(kt_i)\,\delta(\tau-kt_i) \sum_{m=-\infty}^{\infty} x(mt_i+kt_i)\,\delta(t+\tau-mt_i-kt_i) \right\} d\tau$$

or

$$E\{\tilde{x}(t)_+\, \tilde{y}(t)\} =$$

$$\lim_{T\to\infty} \frac{1}{2T}\, t_i^{\,2} \sum_{m=-\infty}^{\infty} \sum_{k=-\infty}^{\infty} y(kt_i)\,x(mt_i+kt_i) \int_{-T}^{T} \delta(\tau-kt_i)\,\delta(t+\tau-mt_i-kt_i)\,d\tau \tag{A-12}$$

Let $T = (2N+1)t_i$. Then the limits of the integrand in (A-12), $-T \le \tau \le T$ can be replaced with $-\infty \le \tau \le \infty$ by limiting the sum over k from -N to +N; that is,

$$E\{\tilde{x}(t)_+\, \tilde{y}(t)\} =$$

$$\lim_{N\to\infty} \frac{t_i^{\,2}}{(2N+1)t_i} \sum_{m=-\infty}^{\infty} \sum_{k=-N}^{N} y(kt_i)\,x(mt_i+kt_i) \int_{-\infty}^{\infty} \delta(\tau-kt_i)\,\delta(t+\tau-mt_i-kt_i)\,d\tau \tag{A-13}$$

The integral in (A-13) can be evaluated using (A-2) and (A-3):

$$\int_{-\infty}^{\infty} \delta(\tau-mt_i)\,\delta(t+\tau-mt_i-kt_i)\,d\tau = \int_{-\infty}^{\infty} \delta(\tau-kt_i)\,\delta(mt_i+kt_i-\tau-t)\,d\tau$$

$$= \delta[-t-(kt_i-mt_i-kt_i)] = \delta(-t+mt_i) = \delta(t-mt_i) \qquad \text{(A-14)}$$

It is also recalled that an ensemble average may be used to compute the crosscorrelation function [11]; thus

$$C_{x_+y}(mt_i) = \lim_{N\to\infty} \frac{1}{(2N+1)} \sum_{k=-N}^{N} y(kt_i)\,x(mt_i+kt_i) \qquad \text{(A-15)}$$

Substituting (A-15) and (A-14) into (A-13) yields

$$E\{x(\tilde{t})_+\, y(\tilde{t})\}$$

$$= \sum_{m=-\infty}^{\infty} t_i\, C_{x_+y}(mt_i)\,\delta(t-mt_i)$$

or using (A-1) and (A-3),

$$E\{x(\tilde{t})_+\, y(\tilde{t})\} = \sum_{m=-\infty}^{\infty} C_{x_+y}(t)\,\delta(t/t_i-m). \quad \text{Q.E.D.}$$

A corrollary to this theorem is that the autocorrelation of a sampled function may be represented by

$$E\{x(\tilde{t})_+\, x(\tilde{t})\} = \sum_{m=-\infty}^{\infty} A_x(t)\,\delta(t/t_i-m) \qquad \text{(A-16)}$$

This may be proved by letting $x(\tilde{t}) = y(\tilde{t})$ in (A-9) and recognizing that $C_{x_+x} = A_x$.

Theorem 2:

The crosscorrelation of a sampled function, $x(\tilde{t})$, and a non-sampled function $y(t)$ is

$$E\{x(\tilde{t})y(t)_+\} = C_{xy_+} \tag{A-17}$$

In words, the fact that one of the terms being correlated is sampled does not alter the form of the crosscorrelation function.

Proof:

Proceeding as in Theorem 1,

$$E\{x(\tilde{t})y(t)_+\}$$

$$= \lim_{T\to\infty} \frac{1}{2T} \int_{-T}^{T} y(t+\tau) \sum_{m=-\infty}^{\infty} x(\tau)\delta(\tau/t_i - m)d\tau$$

or using (A-1) and (A-3)

$$E\{x(\tilde{t})y(t)_+\} = \lim_{T\to\infty} \frac{t_i}{2T} \int_{-T}^{T} y(t+\tau) \sum_{m=-\infty}^{\infty} x(mt_i)\delta(\tau - mt_i)d\tau \tag{A-18}$$

Letting $T = (2N+1)t_i$ and exchanging limits on m and $\tau$ leads to

$$E\{x(\tilde{t})y(t)_+\}$$

$$= \lim_{N\to\infty} \frac{t_i}{(2N+1)t_i} \sum_{m=-N}^{N} x(mt_i) \int_{-\infty}^{\infty} y(t+\tau)\delta(\tau - mt_i)d\tau \tag{A-19}$$

Recalling Eq. (2.3) and recognizing the ensemble average form of the crosscorrelation function, (A-19) leads to

$$E\{x(\tilde{t})y(t)_+\} = \lim_{N\to\infty} \frac{1}{(2N+1)} \sum_{m=-N}^{N} x(mt_i)y(t+mt_i)$$

$$\equiv C_{xy_+} \qquad \text{Q.E.D.}$$

A corollary to Theorem 2 is that the crosscorrelation function of a sampled function $x(\tilde{t})$ and its non-sampled generator, $x(t)$, is the autocorrelation function of $x(t)$. This is proved by substituting $y(t) = x(t)$ in Eq. (A-17); thus,

$$E\{x(\tilde{t})x(t)_+\} = C_{xx_+} = A_x \qquad \text{(A-20)}$$

APPENDIX B

Consequences of the Previous Theorems

The relationship between the PSD, $\tilde{P}_x(f)$, of a sampled function $x(\tilde{t})$ and the autocorrelation function $A_x(t)$ will be developed. The one dimensional forms of Eqs. (2.8) and (2.9) are

$$P_x(f) = \int_{-\infty}^{\infty} A_x(t) e^{-2\pi jft} dt$$

and

$$A_x(t) = \int_{-\infty}^{\infty} P_x(t) e^{2\pi jft} dt$$

The PSD of the sampled function is found from

$$\tilde{P}_x(f) = \int_{-\infty}^{\infty} E\{x(\tilde{t}) + x(\tilde{t})\} e^{-2\pi jft} dt$$

Substituting (A-16) into (B-3),

$$\tilde{P}_x(f) = \int_{-\infty}^{\infty} \sum_{m=-\infty}^{\infty} A_x(t) \delta(t/t_i - m) e^{-2\pi jft} dt$$

Using (A-1) and (A-3),

$$\tilde{P}_x(f) = \sum_{m=-\infty}^{\infty} t_i A_x(mt_i) \int_{-\infty}^{\infty} \delta(t - mt_i) e^{-2\pi jft} dt$$

Recalling Eq. (2.3), (B-5) can be written

$$\tilde{P}_x(f) = \sum_{m=-\infty}^{\infty} A_x(mt_i) e^{-2\pi jfm\, t_i}\, t_i \qquad \text{(B-6)}$$

The inverse relationship is established as follows. Multiply both sides of (B-6) by $e^{2\pi jfp\, t_i}$ and integrate over $-\frac{1}{2t_i} \leq f \leq \frac{1}{2t_i}$. Then,

$$\int_{-1/2t_i}^{1/2t_i} \tilde{P}_x(f) e^{2\pi jfp\, t_i}\, df = t_i \sum_{m=-\infty}^{\infty} \int_{-1/2t_i}^{1/2t_i} A_x(mt_i) e^{2\pi jf(m-p)t_i} df \qquad \text{(B-7)}$$

Letting $z = 2\pi t_i f$

and $dz = 2\pi t_i df$

it can be shown that

$$t_i \int_{-1/2t_i}^{1/2t_i} e^{2\pi jf(m-p)t_i}\, df = \frac{1}{2\pi} \int_{-\pi}^{\pi} e^{z(m-p)}\, dz = \begin{cases} 1, p=m \\ 0, p\neq m \end{cases}$$

Thus, (B-7) leads to

$$A_x(pt_i) = \int_{-1/2t_i}^{1/2t_i} \tilde{P}_x(f) e^{2\pi jfp\, t_i}\, df \qquad \text{(B-8)}$$

Note the important consequence that

$$\overline{x(\tilde{t})^2} = A_x(0) = \int_{-1/2t_i}^{1/2t_i} \tilde{P}_x(f)df \qquad \text{(B-9)}$$

where $\overline{x(\tilde{t})^2}$ is the mean square value of the sampled function $x(t)$.

A very useful equation would define the relationship between the PSD functions of a sampled and unsampled quantity. Eq. (B-3) may be written in the form

$$\tilde{P}_x(f) = F[E\{x(\tilde{t})_+ x(\tilde{t})\}] \qquad \text{(B-10)}$$

From (A-16), (B-10) becomes

$$\tilde{P}_x(f) = F[\sum_{m=-\infty}^{\infty} A_x(t) \ (t/t_i - m)]$$

or using the Borel convolution theorem,

$$\tilde{P}_x(f) = F[A_x(t)] * F[\sum_{m=-\infty}^{\infty} \delta(t/t_i - m)] \qquad \text{(B-11)}$$

where the asterisk represents convolution.
It follows directly from (B-1) that

$$P_x(f) = F[A_x(t)] \qquad \text{(B-12)}$$

It is proved by Papoulis [10] that

$$F\left[\sum_{m=-\infty}^{\infty} \delta(t/t_i - m)\right] = \sum_{m=-\infty}^{\infty} \delta(f - m/t_i) \qquad \text{(B-13)}$$

Combining (B-11), (B-12) and (B-13) gives

$$\hat{P}_x(f) = \sum_{m=-\infty}^{\infty} \int_{-\infty}^{\infty} P_x(f-f')\,\delta(f'-m/t_i)\,df'$$

or

$$\hat{P}_x(f) = \sum_{m=-\infty}^{\infty} P_x(f - m/t_i) \qquad \text{(B-14)}$$